43

Confocal and Multi-Photon Imaging of Living Embryos

Jeff Hardin

INTRODUCTION

By its very nature, developmental biology requires thinking in four dimensions. Not only do embryos change dramatically over time, as the seemingly featureless single-celled zygote is transformed into an embryo with recognizable body axes and organ systems, but this remarkable transformation occurs in three spatial dimensions. The coordinated changes that occur within the developing embryo include carefully orchestrated signaling events, changes in gene expression, and morphogenetic movements, that is, regulated cell divisions and cell movements that sculpt the basic body plan as a recognizable organism emerges.

Non-confocal imaging modalities, such as Nomarski microscopy and widefield epifluorescence, have played a key role in the analysis of whole, living embryos in several important model systems, such as *Caenorhabditis elegans* (Thomas *et al*., 1996; Thomas and White, 2000) and zebrafish and other teleosts (Concha and Adams, 1998). In less transparent embryos, including amphibians such as *Xenopus* (Wilson and Keller, 1991) and avian embryos (Chapman *et al*., 2001; Czirok *et al*., 2002), important work has been done to analyze overall changes in shape of embryos or in microsurgically explanted tissues. However, it is no exaggeration to say that confocal microcopy has been a revolutionary technology in the resurgence of microscopy as a key analytical tool of the developmental biologist. Beginning in the late 1980s and continuing throughout the decade of the 1990s to the present, the development of devices that could capture four-dimensional (4D) datasets of fluorescent molecules within embryos with increasing temporal and spatial resolution has allowed processes progressively deeper within embryos to be studied for the first time. As laser, photomultiplier, and charge-coupled device (CCD) technologies have improved, so has our ability to image large embryos *in situ*, including opaque embryos, such as *Xenopus* and the chick. The impact of confocal microscopy has not been restricted to the specialist; the striking images obtained using confocal microscopy have also transformed how data are presented in the teaching laboratory and classroom.

Despite these successes, challenges remain. Some of these challenges are specific to particular types of embryos, but others are faced by all developmental biologists, no matter which model system they choose. This chapter sets out several of these common challenges, and how developmental biologists are overcoming them as they attempt to bring modern confocal and multi-photon microscopy to bear on key developmental events.

INTO THE DEPTHS: EMBRYOS ARE THICK, REFRACTILE, AND SUSCEPTIBLE TO PHOTODAMAGE

Imaging Embryos Often Requires "4D" Imaging

One of the vicissitudes of imaging living embryos is that they are thick, and their structure is constantly changing. As a result, embryos must often be imaged throughout their thickness and over time. Such 4D imaging entails the collection of a stack of images made at different focal depths along the imaging axis at specified time intervals. Once each three-dimensional (3D) image stack has been collected, the objective is repositioned at the starting position in preparation for the next time point, at which time this cycle is repeated. For typical long-term acquisition experiments involving fluorescent probes detected in living embryos, exposure of embryos to the excitation beam is prevented between time points by a shuttering system, thereby minimizing photodamage to the embryo.[1] Although the details differ, modern commercial confocal, multi-photon, and widefield/deconvolution microscopes all offer acquisition packages that allow for the collection of such 4D datasets.

Four-dimensional datasets of fluorescent specimens acquired using confocal, multi-photon, or widefield deconvolution techniques have several advantages over 4D datasets acquired using transmitted light optics, such as Nomarski microscopy (Thomas *et al*., 1996; Thomas and White, 2000). First, confocal acquisition permits much more refined optical sectioning of the specimen with little contribution by out-of-focus information. For large, thick embryos, this means that events at significant distances from the coverslip can be imaged crisply without contaminating signal from other regions of the embryo. Second, but of equal importance, it is much easier to understand the distribution of the fluorescent

[1] In this chapter, as elsewhere in this book, we assume, that, to a first approximation, photodamage is proportional to the total number of fluorescent signal photons actually excited and that one scan at a power level of 100 μW will do the same damage as 10 scans at 10 μW. This means that one must use much lower levels of excitation in a study requiring many planes per *z*-stack and many time points in the time series. This proportionality may break down at higher power levels that approach singlet-state saturation of the fluorophore where the chance increases that each excitation will produce damage.

Jeff Hardin • University of Wisconsin, Madison, Wisconsin 53706

signal from a sample on the basis of a 3D voxel rendering than to derive any sort of "real" data from a 3D stack of differential interference contrast (DIC) images (for an attempt at the latter, see Heid *et al*., 2002 and Chapter 24, *this volume*).

The Quest for Better Resolution: Aberration and the Challenge of Imaging Thick Embryos

It is common for beginning students of developmental biology to become preoccupied by the dazzling sophistication of modern computer visualization techniques. While they certainly have visual appeal, it is sometime less obvious to students and researchers that optimizing the optical system to get better data can often be more important for imaging embryos than the subsequent use of software to display the raw image data.

Although it may seem obvious to anyone who has tried to image events during embryogenesis, it is worth considering the crucial optical challenge developmental biologists face as they try to capture and analyze dynamic processes during embryogenesis: *embryos are rarely flat.* Indeed, often they are extremely thick along the axis of the light path. For example, *Xenopus* embryos are roughly 1 mm in diameter, and chick embryos are larger still at late stages in development. These distances mean that even in the absence of significant light scattering by the specimen, spherical aberration can be an important constraint on obtaining quality images deep within a specimen (see Chapters 2, 7, and 20, *this volume*, for further details on the effects of spherical aberration). For thick specimens, aberration introduced due to refractive index mismatch between oil-immersion objectives and the aqueous medium is significant. For thin specimens imaged within 5 µm of the coverslip (such as *C. elegans* embryos, in cases where surface features are of interest, or when an explant technique has been used to effectively flatten the specimen), a high numerical aperture (NA) lens (NA = 1.4) is typically the best choice.

The spatial effects of these aberrations have been determined for both confocal and two-photon microscopes, and they can be profound. Mismatch artifacts can affect axial resolution, introduce focal shifts of the image plane, and result in dramatic decreases in image intensity (Hell *et al*., 1993; DeGrauw *et al*., 2002). Such problems may be solved in part by using water-immersion lenses for specimens more than ~10 µm in thickness, although many developmental biologists assume that maximizing numerical aperture by using oil-immersion lenses is the *sine qua non* of high-resolution imaging. For aqueous specimens thicker than ~10 µm, a water-immersion lens with a lower NA outperforms a high-NA oil-immersion lens.

Embryos Are Highly Scattering and Refractile Specimens

Light scattering is often fairly acute, even in the case of relatively small embryos, such as *C. elegans* and *Drosophila* (~25 µm and 200 µm along their short axes, respectively). Within the cells of such embryos particles that are significantly smaller than the excitation and emission wavelengths contribute to Rayleigh scattering (see Chapter 21, *this volume*), which depends inversely on the fourth power of the wavelength. Consequently, such scattering can be lessened by using longer excitation wavelengths; for strongly scattering specimens, two- or multi-photon imaging can further reduce scattering of excitation photons (see below). Unfortunately, there are other major sources of scattering in embryos. The cells of early embryos typically have yolk platelets or other highly refractile granules within the cytoplasm that deflect both excited and emitted light. Moreover, most embryos are spherical; the curvature of their outer surface is also a major source of refraction.

Imaging Embryos Involves Inherent Trade-Offs

Imaging thick embryos typically means a trade-off between lateral and axial resolution and signal strength on the one hand, and working distance and field diameter on the other. Typical epifluorescence objectives effectively act as both condenser for incident light passing through the excitation filter and off the dichroic mirrors, as well as serving as the objective lens that collects and focuses the photons emitted from the specimen. As magnification increases, signal/area in the image decreases, but this is counterbalanced by the higher NA of the objective. For high-resolution imaging, developmental biologists typically seek to maximize numerical aperture while keeping the magnification low enough to permit them to see the whole embryo or at least the part of it of most interest.

Although the discussion of contrast is complex, it is clear that for fluorescent specimens, contrast and effective resolution of structures labeled with fluorophores are linked (for further discussion of the issues relating the contrast transfer function, CTF, see Chapters 2, 4, 8, and 35, *this volume*). At a simple level, contrast is determined by the ratio of local intensity differences in the specimen to the local average intensity in the image, $\Delta I/I$. To a first approximation, the local emission intensity difference for typical applications in embryos is proportional to the local concentration of fluorophores above background. Moreover, as the emitted signal is proportional to the local fluorophore concentration, developmental biologists usually seek to increase the local signal as much as possible by increasing staining intensity or the concentration of green fluorescent protein (GFP)-tagged molecules per unit volume. Here again, however, there are often trade-offs because excessive labeling achieved by over-expression of a fluorescent protein can interfere with cellular function.

Although increasing the illumination intensity increases the fluorescent signal, dynamic imaging of fluorophores within living embryos requires multiple exposures to the excitation light, so developmental biologists can rarely afford to use high illumination intensity. Indeed, they are acutely aware that this simple solution typically results in dead embryos! Therefore, a balance must be sought between the intensity of the illumination and a host of other factors important to achieving quality images. Because embryos are so thick and their cells are moving in four dimensions, multiple focal planes must be acquired at each successive time point. While such 4D information is powerful, it requires exposing the region of interest to more laser light than that required for viewing flat cells in culture. Thus, minimizing exposure to the excitation wavelength is a key factor in maintaining the viability of embryos during 4D experiments.

The photobleaching that accompanies repeated observation in 4D experiments also complicates image quantification. If photobleaching is not too severe, it is sometimes possible to normalize the signal from bleached specimens using a reference fluorescent signal, but this only works if the specimen and the reference bleach at the same rate. In general, the best solution to this problem is reducing the power of the excitation beam as much as possible. Although multi-photon microscopy has the advantage that fluorophore is excited only within a small volume near the focal plane of the objective, this advantage must be balanced against the fact that some dyes bleach more rapidly per photon emitted with two-photon than with single-photon excitation. Clearly, multi-photon

excitation is the imaging modality of choice if bleaching is a serious concern and the stained thickness of the specimen is high.

Common Themes in Living Embryo Imaging Have System-Specific Solutions

Although developmental biologists have developed several ways to address challenges common to imaging all living embryos, given the dramatic differences in the basic cell biology between the most common model organisms, solutions are typically specific to a particular model system. Rather than reviewing the virtues and drawbacks of each model system and describing highly detailed techniques for solving particular imaging issues in each one, the remainder of this chapter will focus on examples of ways in which developmental biologists are meeting the challenges of long-term imaging of fluorescent molecules deep within living embryos.

Before reviewing such examples, several generalizations about the apparatus and dyes useful in imaging living embryos are in order. First, there is a necessary element of empiricism in determining which type of microscope is necessary for a particular fluorophore in a particular embryonic context. Currently, standard laser-scanning confocal systems still dominate over other types of imaging equipment, and thus a significant amount of live embryo imaging is being attempted — and successfully performed — on such equipment. While it is true that there are advantages to multi-photon microscopy in terms of depth of penetration into a specimen and, in some cases, viability, laser scanning suffices for a wide variety of imaging situations. Depending on the density of fluorophore labeling and the nature of the tagged moiety, the majority of experiments have been performed using rather unremarkable equipment, such as a Bio-Rad 1024 or similar laser-scanning confocal apparatus.[2] Although such experiments sometimes suffer from limited image acquisition speed, live imaging of embryos using laser-scanning confocal microscopy has been extremely successful.

A second general consideration is that the way in which a fluorophore affects viability is crucially dependent on the macromolecule to which it is attached. For example, in our laboratory, transcriptional reporters that drive the expression of GFP in the cytosol can withstand irradiation at 10% to 30% power of the 488 line on a conventional Bio-Rad 1024 microscope with a krypton/argon (Kr/Ar) laser for many minutes to hours, whereas imaging embryos expressing a GFP-tagged protein found at epithelial junctions under the same imaging conditions either kills the cells or renders them unable to develop properly (J. Hardin, unpublished observations).

Third, even if the problems of working with thick, refractile embryos can be at least partially solved by using confocal or multi-photon microscopy, developmental biologists still need ways to specifically label interesting features in living embryos. In some cases, they wish to highlight multiple structures simultaneously within the same specimen, and this requires delivering multiple fluorophores to specific sites within embryos. Although not specific to confocal and multi-photon microscopy, specific labeling strategies are nevertheless a key adjunct to these imaging technologies. In essence, this is a continuation of the microscopist's quest to increase specimen contrast, no matter what imaging modality is being used.

[2] Interested readers are urged to consult reviews describing methods of confocal and multi-photon imaging in specific model systems. These include methods for imaging *Xenopus* (Bement *et al*., 2003), zebrafish (Cooper *et al*., 1999), *Drosophila* (Wood and Jacinto, 2004), and *C. elegans* (Mohler, 1999) embryos.

DEALING WITH DEPTH: STRATEGIES FOR IMAGING THICK SPECIMENS

Avoiding the Thickness Dilemma: Going Small

Model systems in developmental biology are often chosen to avoid the thickness dilemma. For example, *C. elegans* embryos are only ~25 µm thick along their dorsoventral axis, commonly used echinoderm embryos are only 80 to 120 µm in diameter, and *Drosophila* embryos are ~200 µm along their dorsoventral axis. Zebrafish are at the limits of penetration via multi-photon microscopy (~600 µm in diameter), but because most relevant events occur near the surface, they too are effectively fairly flat. As a result, there are many examples in which embryos from these model systems are imaged in 4D using confocal and multi-photon techniques. These include the imaging of GFP-tagged proteins in *Drosophila* embryos during dorsal closure and germ band extension, processes that take several hours (Wood and Jacinto, 2004), cell migration in the epidermis during morphogenesis of *C. elegans* embryos (Mohler *et al*., 1998; Heid *et al*., 2001), events during fertilization and subsequent early development of echinoderm embryos (Terasaki, 1998), and 4D analysis of morphogenesis in zebrafish embryos (Cooper *et al*., 1999).

Grazing the Surface: Superficial Optical Sections Are Often Sufficient

While many model systems are small in size, some are at the limits of standard confocal microscopy. For example, *Xenopus* embryos are a full 1 mm in diameter. Moreover, because their dense yolk platelets scatter light, imaging deep into the interior of amphibian embryos is an acute technical challenge. One simple strategy is to concede that imaging events deep within the embryo is not possible, and to focus on what can be seen near the surface of the oocyte, fertilized egg, or early zygote. Such events can be imaged extremely well using a single-beam confocal microscope and a variety of labeling techniques, including fluorescent dextrans, lipophilic dyes, fluorescently labeled proteins or antibodies introduced via microinjection, or by expressing GFP-tagged proteins following injection of mRNA (Bement *et al*., 2003). A montage from a representative dataset from a *Xenopus* oocyte is shown in Figure 43.1(A), which shows the redistribution of active Rho and actin during the closure of a wound in a *Xenopus* oocyte. Such imaging experiments often involve 4D imaging, although because of the high speed of the movements involved, only a few optical sections (<10) can typically be recorded at each time point (Bement *et al*., 2003). To image events deeper within the embryo, however, additional techniques must be employed.

Up from the Deep: Explants Can Reduce the Thickness of Specimens Dramatically

In some cases, imaging the surface of thick embryos is simply not sufficient. For example, during gastrulation, cells move large distances within the interior of the embryo. In the case of the relatively opaque *Xenopus* embryo, it is simply not feasible to image such tissues directly, because they may be several hundred

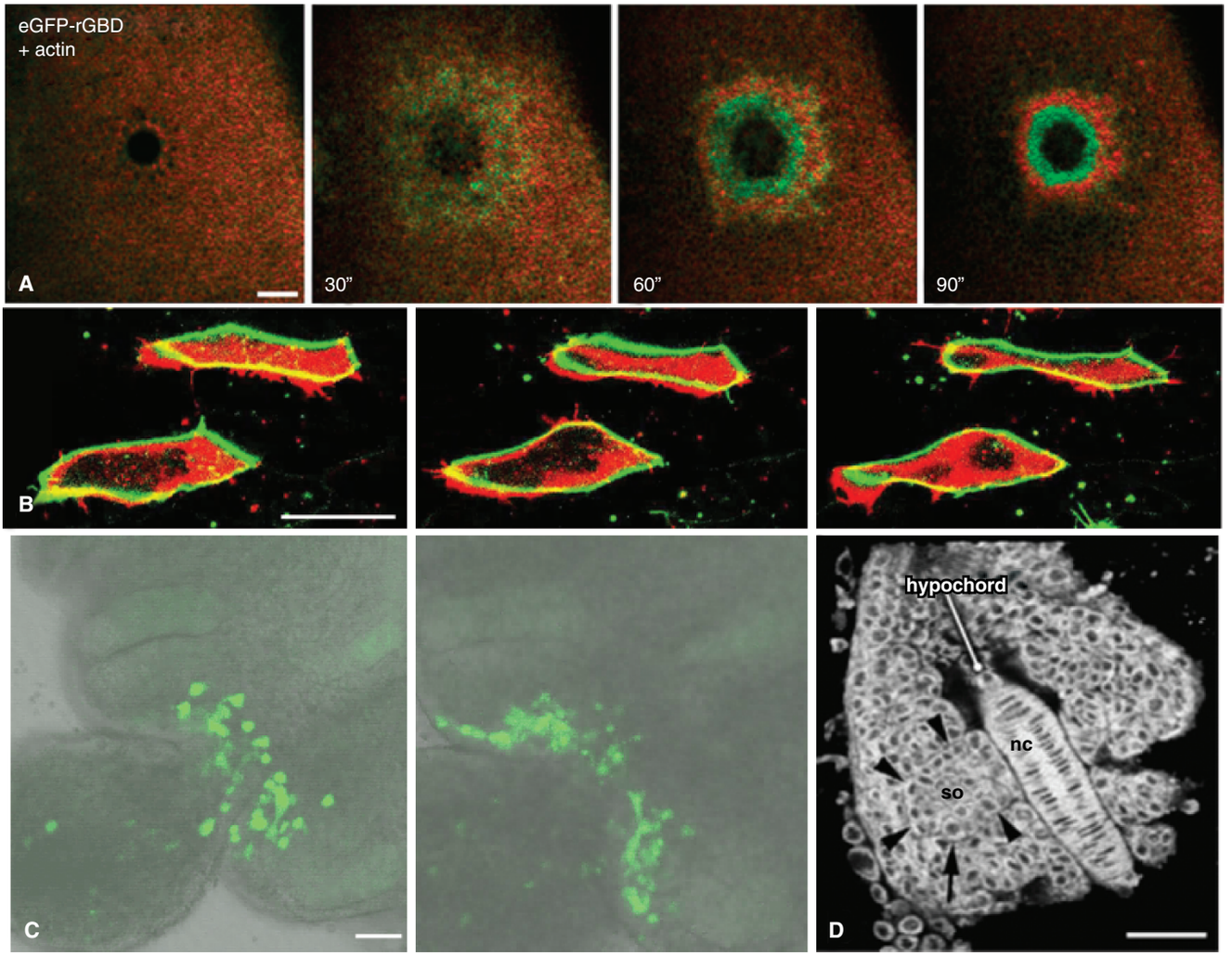

FIGURE 43.1. Strategies for imaging very thick embryos. (A) A 4D study of events on the surface of a *Xenopus* oocyte. Shows wound closure in a *Xenopus* oocyte expressing a protein that binds active Rho fused to eGFP (eGFP-rGBD; green) and Alexa-568 labeled actin (red) imaged using a Bio-Rad 1024 CLSM. Bar = 15 µm. Times indicated are in seconds. (B–D) Imaging events in an explant. (B) Frames from a fluorescence confocal movie in which intercalating *Xenopus* mesodermal cells are visualized at two levels: the surface of the explant (red channel) and 5 µm deep in the tissue (green channel). Cell membranes are labeled with GAP-43::GFP. Bar = 50 µm. (C) Frames from a confocal time-lapse sequence showing migration of primordial germ cells (PGCs) in a slice from a stage E9.5 embryo expressing Oct4ΔPE::GFP, imaged at 7 min intervals using a Zeiss LSM-510 CLSM. PGCs migrate into the genital ridges. Data taken 455 min later. Bar = 50 µm. (D) Ventral view of an explanted zebrafish tail rudiment (14-somite stage) mounted ventral side down using plasma clot immobilization vitally stained with Bodipy 505/515 imaged using a Bio-Rad MRC600 CLSM. The notochord and a neighboring somite (so, *arrowheads*) are visible. An individual somitic mesodermal cell (*arrow*) is in mitotic prophase. Scale bars = 50 µm. [(A) is from Benink and Bement (2005); (B) is from Keller (2002); (C) is from Molyneaux and colleagues (2003); (D) is from Langenberg and colleagues (2003), used by permission.]

micrometers from the surface, and light scattering is severe at that depth. In this case, a better approach is to isolate the tissue of interest using microsurgery. By isolating a sheet of tissue that is relatively thin along the imaging axis, the embryo has in effect been flattened. Such an embryo, expressing a membrane-localized GFP, is shown in Figure 43.1(B). Although 4D datasets must still be acquired to capture the relevant aspects of cell motility in this specimen, the explant is sufficiently transparent that one can acquire *z*-stacks that encompass its entire thickness (Keller, 2002). Other similar techniques have been used to render tissues in other large embryos amenable to 4D analysis. These include analysis of primordial germ cell migration in mouse embryos (Molyneaux *et al.*, 2003) [Fig. 43.1(C)] and the microsurgical removal of the yolk cells from post-gastrula stage zebrafish embryos (Langenberg *et al.*, 2003) [Fig. 43.1(D)].

Multi-Photon Microscopy Can Penetrate More Deeply into Specimens

Multi-photon laser-scanning microscopy (MPLSM) has gained wide acceptance as an alternative to standard laser-scanning confocal microcopy because it has several potential advantages over CLSM for live imaging of embryos. MPLSM excites fluorescence using a series of short, high-energy pulses of near-infrared (NIR) photons from a mode-locked laser. At the very high photon densities that result, two or more photons can be absorbed simultaneously to excite a single fluorophore, which then returns to the unexcited ground state by a standard fluorescence emission event. In the case of two-photon excitation, the excitation wavelength is set to roughly twice that used for single-photon (i.e., normal) excitation of the same fluorophore (see Chapter 28, *this volume*, for a

detailed description of multi-photon microscopy). Although theoretical calculations and measurements of actual point spread functions indicate that the axial resolution in MPLSM is about 40% lower than in CLSM (Jonkman and Stelzer, 2002), MPLSM has two key advantages for live embryo imaging experiments.

As the two-photon excitation probability is proportional to the square of the local beam intensity (see Chapter 28, *this volume*), given the conical shape of the standard excitation beam, the probability of excitation varies as the inverse fourth power of the distance from the focal plane. The result is that photons are absorbed only in a very small volume centered on the plane of focus. As long as no regions of the specimen cause single-photon absorption of light at this wavelength, it is essentially transparent to the incident laser light. This eliminates photobleaching and photodamage caused by excitation of fluorophores above and below the plane of focus.

The resulting improvements in viability can be quite dramatic. For example, hamster embryos imaged with CLSM using the mitochondrial marker Mitotracker Rosamine did not develop to the blastocyst stage, whereas similarly labeled embryos imaged using MPLSM at 1047 nm were capable of late fetal development and even birth (Squirrel *et al*., 1999). In our own laboratory, *C. elegans* embryos expressing a GFP-tagged junctional protein survive for 30 to 90 min when imaged using a Bio-Rad 1024 CLSM at low power (10%; J. Hardin, unpublished observations) but the same embryos can be imaged for many hours using MPLSM.

Second, the longer wavelength of the MPLSM excitation beam scatters less and is not absorbed by fluorophores located above the focus plane. These characteristics permit it to excite fluorophores deep inside the specimen (Fig. 43.2), in some transparent embryos such as zebrafish, up to ~500 µm from the surface (Megason and Fraser, 2003). In addition, because multi-photon excitation generates significant signal only at the plane of focus, no pinhole is required to detect an image resolved in three dimensions. One must simply detect light that was emitted at a specific time. As a result, one can used non-descanned detection, a process in which even fluorescent light that had suffered multiple scattering events can still contribute to the image as long as it reaches a photodetector. For thick specimens, this can increase signal level by a factor of up to 3× (Centonze and White, 1998).

Although MPLSM can be superior to CLSM for many applications, there are several issues that can make MPLSM less than optimal. First, the typical MPLSM device is expensive, placing it out of reach of most individual laboratories. In contrast, individual labs can often afford disk-scanning confocal microscopes, a factor that is particularly important for live embryo studies, which often monopolize microscope time. Second, for certain fluorophores, for example, those that emit in the red portion of the visible spectrum, the wavelengths needed to generate a two-photon event are longer than those produced by the titanium : sapphire (Ti : Sa) lasers commonly used in commercial MPLSM devices. For such dyes, Nd : YLF lasers, which emit at 1047 nm, are very effective (Mohler *et al*., 1998; Squirrell *et al*., 1999; see also Fig. 43.9), but may not be readily available. Third, some pigments, such as those found in living *Xenopus* embryos, absorb the NIR light used to excite GFP and other green-emitting fluorophores by two-photon events. Such absorption usually causes severe damage (see Chapter 38, *this volume*).

Although MPLSM is clearly a tremendous tool in the arsenal of the developmental biologist, in light of these caveats, it is

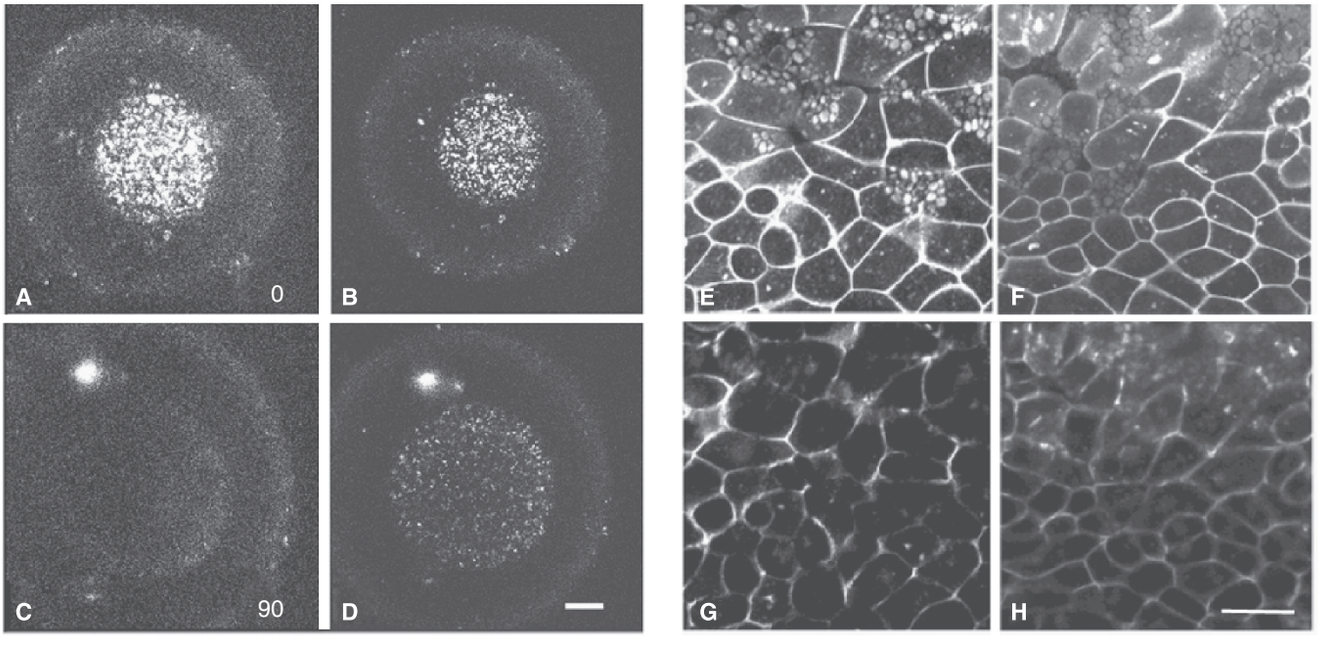

FIGURE 43.2. Multi-photon microscopy is useful for penetrating more deeply into embryos. (A) A bovine embryo stained with Mitotracker rosamine to detect mitochondria, imaged via confocal microscopy (left; 3.5 W of 532 nm light) and by multi-photon microscopy (right; YLF laser, direct detection, 10 mW of 1047 nm light), using a Kalman three-collection average. Mitochondria are roughly uniformly distributed in such embryos. Mitochondria cannot be visualized using the CLSM, but are clearly visible using the MPLSM. Bar = 20 µm. (B) Comparison of multi-photon and confocal microscopy for imaging morphogenesis in the *Xenopus* embryo. Images of GAP-43 :: GFP fusion protein in developing *Xenopus* embryos were acquired with the same objective lens using CLSM (Nikon PCM 2000) and TPLSM systems (Bio-Rad MRC 600 scan head, with Ti : Sa laser at 870 nm). Less detail is evident deeper in the specimen with CLSM. Bar = 50 µm. [(A) is from Centonze and White (1998); (B) is adapted from Periasamy and colleagues (1999), used by permission.]

usually wise to try standard confocal imaging first before assuming that MPLSM is necessary for a particular specimen. Our own laboratory has found, for example, that GFP-tagged proteins can usually be imaged in living *C. elegans* embryos with disk-scanning or standard CLSM; on the rare occasions that the image series must proceed for many hours and many focal planes must be acquired, MPLSM remains the method of choice.

Selective Plane Illumination Can Provide Optical Sectioning in Very Thick Specimens

Originally developed by Voie *et al.* (1993) and more recently improved by Stelzer and colleagues (Huisken *et al*., 2004), selective plane illumination microscopy (SPIM; Fig. 43.3), involves a strategy akin to that achieved in nonlinear (two- and multi-photon) microscopy, that is, fluorescence is only excited in a narrow plane perpendicular to the imaging axis (see Chapter 37, *this volume*). A cylindrical lens is used to focus laser light into a light sheet that illuminates only a thin slice of material. In the current configuration, a specimen is embedded in an agarose capsule, and the entire specimen is moved within a bath of liquid. Because only the focal plane being observed is illuminated, the SPIM has similar advantages to MPLSM: far fewer excitations are produced during the acquisition of a 3D dataset. Unlike MPLSM, however, the signal is recorded on a high quantum efficiency CCD camera. These features make SPIM well suited to imaging specimens up to a millimeter in size (see also Chapter 37, *this volume*).

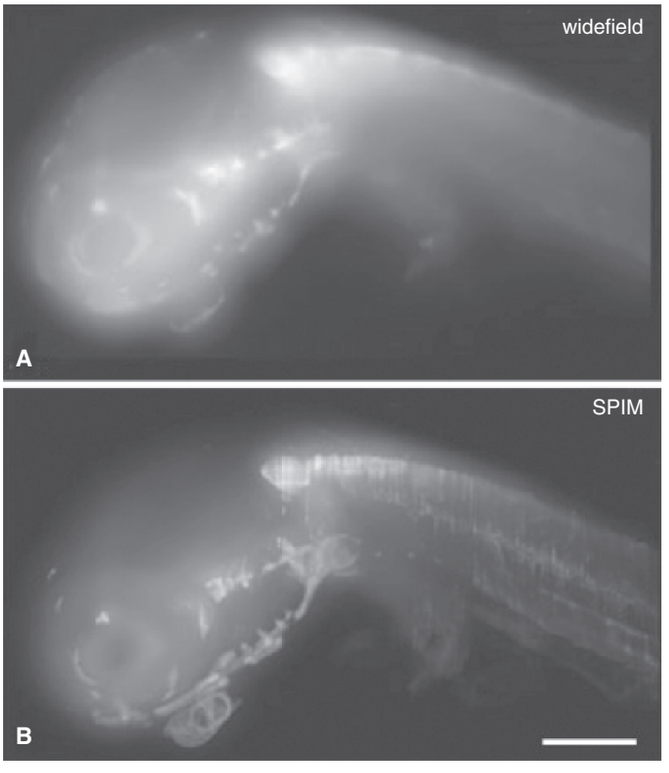

FIGURE 43.3. Selective-plane illumination (SPIM) can optically section huge embryos. A lateral view of a medaka embryo imaged with SPIM by two different modes of illumination. (A) The sample was illuminated uniformly, that is, without the cylindrical lens, as in a conventional wide-field microscope. (B) In contrast, selective plane illumination results in optical sectioning. Bar = 500 μm. [From Huisken and colleagues (2004), used by permission.]

In analogy to the pinhole setting on a standard laser-scanning confocal microscope, the axial resolution in SPIM depends on the thickness of the light sheet, which depends in turn on the working aperture of the cylindrical lens and ranges from 1 μm to 6 μm. This performance can be improved by obtaining additional 3D stacks after rotating the specimen, a process that can provide isotropic resolution down to about 1 μm.

Despite these impressive results, SPIM is still an emerging technology. The current device relies on embedding specimens in low-melting-point agarose, which does not appear to affect the development of fish and *Drosophila* embryos (Huisken *et al*., 2004). Our laboratory has shown that *C. elegans* and sea urchin embryos embedded in agarose also develop surprisingly well (J. Hardin, unpublished observations), suggesting that such embedment may not be a serious limitation. However, as agarose embedding imposes a mechanical impediment to the normal development of those embryos whose overall shape changes dramatically during the period of observation, other specimen stages may have to be developed to accommodate these specimens. In addition, SPIM cannot currently achieve spatial resolution comparable to confocal or multi-photon imaging. Nevertheless, the fact that SPIM has the resolution to identify individual cells in the context of embryos up to 1 mm thick makes it likely that it will become a useful addition to the arsenal of imaging techniques at the disposal of the development biologist.

Deconvolution and Other Post-Acquisition Processing

Widefield deconvolution has typically not been as widely used for imaging whole embryos as have confocal and multi-photon techniques. However, widefield acquisition, followed by post-acquisition deconvolution, can yield images comparable in quality to confocal or multi-photon datasets (Paddy *et al*., 1996) [Fig. 43.4(A,B)]. In deconvolution microscopy, a conventional epi-fluorescence microscope with attached CCD camera, shuttering system, and focus motor is used to capture a 4D dataset. The dataset is subsequently processed to remove out-of-focus contributions to the image at each focal plane (see Chapters 23, 24, and 25, *this volume*, for a detailed discussion of the merits of various deconvolution algorithms that is beyond the scope of this chapter).

Deconvolution has been used less frequently for imaging living embryos for several reasons. First, because the computations involved are extensive, there is no immediate visual feedback regarding the deconvolved image. This immediacy often has a significant psychological effect on the developmental biologist and may help her to guide the experimental procedure. Second, the success of deconvolution is limited by the noise level in the recorded image data. This noise is primarily Poisson noise, and the Poisson noise associated with the measurement of light away from the focus plane is particularly troublesome. Consequently, deconvolution works best when the fluorescent structures are confined to a relatively thin layer of the specimen. Finally, in studies that concentrate on imaging only a single plane over time, confocal and multi-photon imaging are both faster and less damaging to the specimen.

Despite these caveats, widefield/deconvolution microscopy has several advantages for imaging embryos. First, excitation wavelengths are not limited by available laser lines; deconvolution microscopes use standard fluorescence filter sets, and so they can easily visualize many common fluorophores, such as the cyan and yellow variants of GFP.

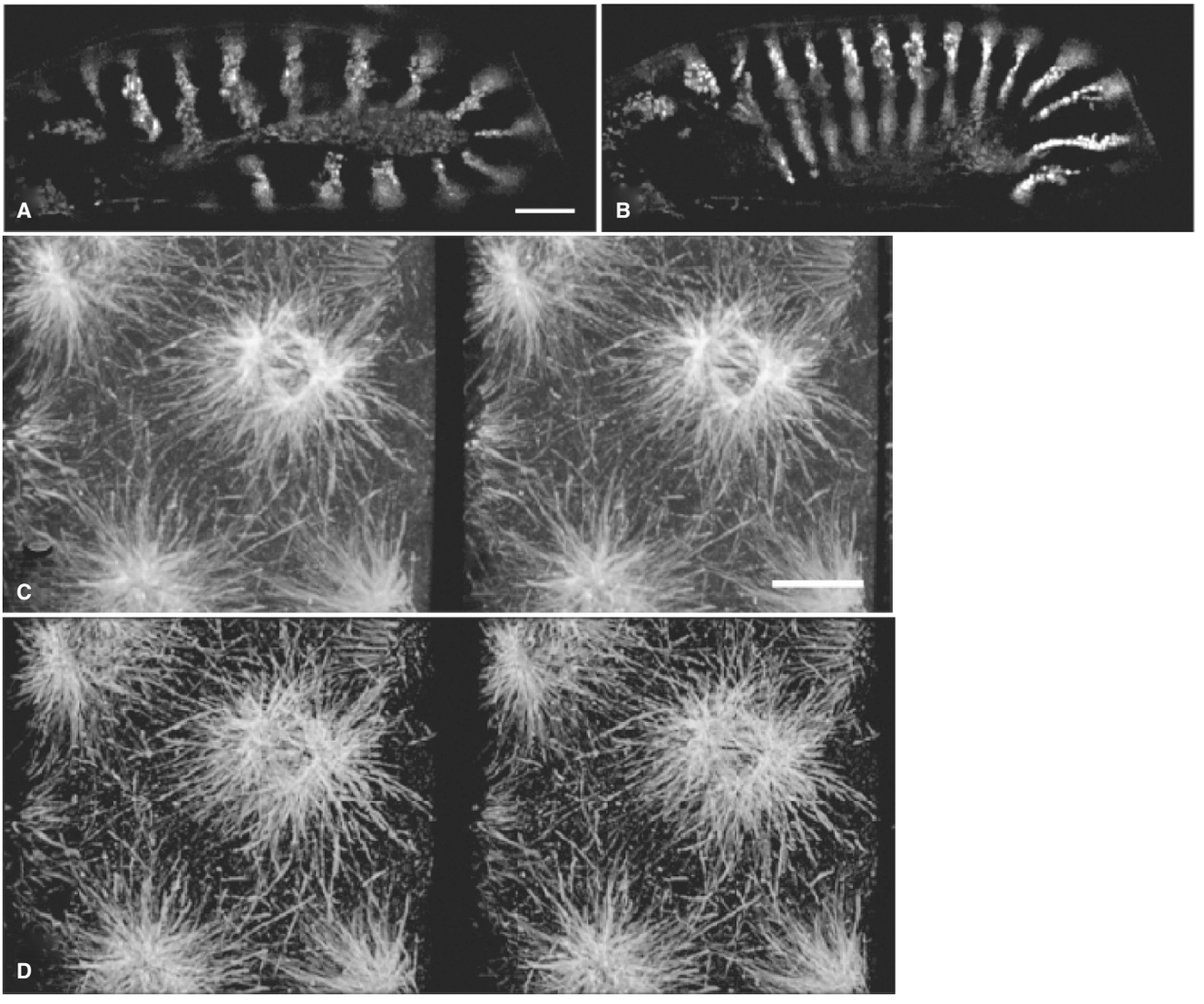

FIGURE 43.4. Deconvolution microscopy can improve optical sectioning of embryos. (A, B) Frames from a time-lapse movie of germ band retraction in a *Drosophila* embryo expressing an *Engrailed:: GFP* reporter, which localizes to nuclei in specific subdomains within each of 14 segments in the embryo, obtained using a DeltaVision deconvolution system. Fine details of the expression pattern are well defined. Bar = 50 µm. (C, D) Stereo-pair images of immunostaining to reveal microtubule distribution in a syncytial stage *Drosophila* embryo imaged using a Bio-Rad MRC-600 LSCM (C), and the same dataset after multiple rounds of deconvolution (D). Fine details within the mitotic spindle regions are visible after deconvolution that were poorly defined prior to deconvolution. Bar = 10 µm. [(A, B) Courtesy of I. Davis, University of Edinburgh. (C, D) Courtesy of G. Odell, University of Washington.]

Another purported advantage of deconvolution microscopy is its claim to cause less photodamage than confocal microscopy when producing an image of a given quality. If true, this difference can probably be traced to the fact that the arc lamps used in widefield epifluorescence produce lower intensity excitation light, and to a lesser extent, because all of the emitted light returned through the optical path reaches the camera (Hammond and Glick, 2000) (see also Chapter 39, *this volume*).

As with most other important parameters for live embryo imaging, the best approach is probably an empirical one. Performing a "test drive" of an expensive imaging system can save time and significant financial resources. Sometimes, the best way to take such a test drive in which living specimens are viewed on a variety of microscopes over a relatively prolonged period is to attend one of the many short courses offered on the topic.

Deconvolution has another important use: it can almost always improve the appearance and accuracy of 4D datasets acquired using confocal or multi-photon imaging [Fig. 43.4(C,D)]. Several studies have shown that postprocessing of confocal and multi-photon stacks using deconvolution can significantly improve their *z*-resolution (Periasamy *et al*., 1999), which is at least 4× lower than their *xy*-resolution, even when using a high-NA lens (Jonkman and Stelzer, 2002).[3] Of more importance for studying living embryos is the fact, that because Nyquist sampling spreads the signal from a single point over about 100 voxels, 3D deconvolution has the effect of averaging the data over about 100 voxels. This greatly reduces the effects of Poisson noise, thereby allowing one to use much lower excitation intensity (see Chapter 19, *this volume*, for 3D data collected using only 50 nW of laser power, and Chapter 25, *this volume*, for more on deconvolving confocal and multi-photon data).

[3] Three times worse for oil, NA 1.4 and 4× for water, NA 1.2. *z*-resolution is proportional to $1/(NA)^2$.

Deconvolution can be especially useful for confocal datasets of living embryos as these are often collected with the pinhole opened somewhat to increase signal. While this compromise increases the total signal and reduces Poisson noise, it also reduces the resolution in the *z*-dimension significantly, and so postprocessing may provide a significant improvement in *z*-resolution as well as signal-to-noise ratio (see Chapter 22, *this volume*). Likewise, 3D datasets from disk-scanning confocal microscopes, which have inherently less resolution along the imaging axis than CLSM, can typically benefit from deconvolution. Here again, however, whether such gains are worth the cost in computation time and effort can only be determined empirically.

STRIVING FOR SPEED: STRATEGIES FOR REDUCING SPECIMEN EXPOSURE

Simple Solutions: Reducing Image Dimensions, Increasing Slice Spacing, and Scan Speed

Two concerns motivate the need for increasing the acquisition speed when imaging embryos. First, rapid cellular events, such as cortical granule release, transport of cellular components along microtubules, and responses to wounding, occur so fast that there simply is not time to acquire finely spaced *z*-stacks of full-field images at maximal resolution. Second, and perhaps more importantly, as exposure to the scanning beam is proportional to the number of images acquired, acquiring more images/second means that the specimen is damaged more rapidly. As a result, the speed with which images can and should be collected must be tailored to each new situation empirically.

From the technical point of view, the speed at which one can acquire images is limited by the rate at which photons are emitted by the specimen: if more frames must be imaged, more photons are needed. The rate at which photons are produced is proportional to the concentration of fluorophore in the focal volume and the intensity of the light striking this volume. Although each of these parameters can be increased, neither can be increased arbitrarily. More laser power will produce additional signal (and additional photodamage!) only until one approaches the power level that produces singlet-state saturation.[4] This saturation limit can only be avoided by using a disk- or line-scanning confocal in which the excitation light is distributed either among an array of many individual points or among a similar number of points arranged to form a line (see Chapter 10, *this volume*).

Of course, the signal must not only be produced, it must also be detected. For this reason, high-speed imaging is also constrained by the quantum efficiency and read noise of the photodetector (a factor that will be discussed below in the context of the development of a new photodetector, the electron-multiplier CCD, or EM-CCD).

Another instrumental constraint is the speed of the scanning system. Single-beam systems that rely on galvanometers to scan the beam are limited to at most 8 k/line/s or about 16 frames/second if the raster size is 512 × 512, while those employing acousto-optical scanners move about 5× faster. On the other hand, the maximum scan rate of disk scanners, which have over a thousand beams in the field of view at any one time, is thousands of frames/second, and is limited chiefly by the vibration produced by the rotating disk. Of course, to collect 3D data one must also scan in the *z*-direction, and whether this is accomplished by moving the specimen or the objective, maximum *z*-scan rates are often limited by the deflection of the specimen slide or coverslip by the forces transmitted through the immersion medium.

The final limit imposed by the acquisition hardware is the rate at which the signal from each pixel can be read out and digitized. On systems utilizing detectors based on advanced CCDs, this is currently about 35 megapixel/s, but if these devices do not employ EM-CCD techniques, the read noise becomes substantial (~±50 electrons/pixel). Although it is possible to digitize the output of a photomultiplier tube at even higher clock speeds, as noted above, this is of little assistance if the dye in the voxel being interrogated is in singlet-state saturation.

A final limitation to consider is the size of the embryo in the *x*- and *y*-dimensions. For some embryos, such as later-stage chick embryos, the region of the embryo that must be imaged constrains acquisition speed. If the linear dimensions of the embryo in the *xy*-plane are large (in the case of a chick embryo, e.g., these dimensions can easily exceed 1 mm), then it may be necessary to image multiple *xy*-sectors. These sectors would then have to be joined into a seamless montage. While semi-automated methods (Beck *et al*., 2000) and fully automated (Czirok *et al*., 2002) methods are becoming available for such montage construction, the initial acquisition of multiple sectors is clearly an additional possible constraint on speed of acquisition and, hence, specimen exposure.

Within the constraints of the limitations listed above, a variety of other parameters can be reduced to optimize data acquisition. These include (1) the number of focal planes acquired at each time point; (2) the number of lines imaged; (3) the time required to build up an acceptable image of the specified *xy*-area in each focal plane; and (4) the interval between the acquisition of each *z*-series. The time required for an "acceptable" image will depend on the type of apparatus. In the case of laser-scanning confocal microscopes, the time required per focal plane will depend on the scanning speed and the number of scans integrated to build up the final signal. Here again, the intensity and contrast of the signal in the specimen will dictate the number of focal planes and the sampling interval and the investigator may have to change several parameters to achieve a satisfactory result. For example, when imaging *C. elegans* embryos in typical 4D experiments in our laboratory using a Bio-Rad 1024 CLSM or a Bio-Rad 1024 scan head for descanned multi-photon imaging, we often use a 1024 × 1024 *xy* pixel box size using the "slow" scan setting, with 30 focal planes 0.5 µm apart collected over a period of ~180 s. This is possible because stacks need only be acquired at 3 to 5 min intervals. In contrast, to image actin coat assembly around exocytosed cortical granules in *Xenopus* oocytes, 15 focal planes must be acquired, and sampling intervals need to be 5 to 10 s. This necessitates a much smaller box size (256 × 256 or 128 × 128 pixels) and higher scan speeds (Bement *et al*., 2003).

When speed is at a premium, single fast scans can often yield acceptable results, especially if a Gaussian filter is applied to the resulting 2D images. Acquiring single fast scans and deconvolving the resulting 3D images will also enhance the signal-to-noise ratio substantially (Jeff Hardin, unpublished observations). In the case of widefield deconvolution or disk-scanning confocal microscopy, the time needed to acquire an image typically represents the time required to integrate sufficient signal on the CCD camera.

[4] In the small spot produced by a high NA oil lens, this occurs for most dyes at about 1 mW. Because a 10× NA 0.5 objective will produce a spot ~3× larger in diameter and 10× larger in area, the same dye would now saturate at 10 mW. In addition to issues regarding saturation itself, there is reason to believe that the bleaching rate/emitted photon increases as one operates closer to saturation (see Chapters 38 and 39, *this volume*).

A final constraint on the speed of acquisition of a *z*-stack involves the eventual display of the collected data in 3D. The process of calculating and displaying renderings of 3D microscopical datasets is complicated by the fact that the resolution in the *z*-direction is always substantially less than that in the *x*- and *y*-directions. The interplane spacing is usually 3× to 4× larger than the *xy*-pixel dimension, and this causes a problem for 3D voxel-rendering algorithms that assume that voxel dimensions are the same in all three dimensions.

There are three solutions to this problem: duplication of slices, interpolation of slices, and collection of more data. The simplest solution involves duplicating the raw data three or four times to fill in the missing planes. This process is fast and restores the proper proportions; however, it makes the resulting images look like a stack of coins and, if the image stack is retained in memory, requires significantly more RAM. The second solution is to derive the missing planes from the measured planes by 2D or 3D interpolation. This process makes the rendering less blocky, but suffers from similar RAM constraints, and also requires significant computer processing time. Finally, one can simply collect data from more planes in the first place, perhaps collecting single-scan images at four focus positions where, to satisfy Nyquist sampling, one would be justified in collecting the Kalman average of four scans over a single plane. Because it avoids additional processing steps, this last solution is the one we most often employ, even thought it entails increased exposure of the embryo to the excitation beam.

Disk-Scanning Confocal Microscopy Allows High-Speed Acquisition

As mentioned above, multi-point confocal microscopes that employ Nipkow disk-scanning technology are another option for increasing data acquisition speed. Because the Yokagawa scan head combines laser excitation with an array of microlenses to force more light through each pinhole in the disk, a high rate of signal production is possible. Because the intensity in each spot is far from singlet saturation and because the effective quantum efficiency of the CCD is higher than that of the photomultiplier tube, disk scanners seem to produce little photobleaching while recording sufficient signal to perform high-quality 4D experiments.

The literature is replete with examples of the use of Yokagawa-based systems for imaging embryos of *C. elegans* (Oegema *et al*., 2001; Cockell *et al*., 2004) and *Drosophila* (Bloor and Kiehart, 2002; Grevengoed *et al*., 2001) in particular. Such microscopes also offer the advantage that the confocal image can be viewed directly, by eye, in real time (see Chapter 10, *this volume*, for an extensive discussion of Yokagawa-based systems and other related technologies).

For the developmental biologist, such systems are an inexpensive alternative to CLSM, and provide many of the benefits of more elaborate technologies, such as multi-photon microscopy. Because disk-scanning systems use an off-the-shelf focus motor, CCD, filter wheel, and shutter components, commercial imaging packages can be used to drive data acquisition. For some laboratories, this may be an advantage compared to the proprietary software that ships with some of these units, especially if they are already using such a software package for other imaging tasks. Although on thick specimens, disk-scanning systems are significantly inferior to CLSM in their optical sectioning capabilities, post-acquisition deconvolution can be an extremely useful adjunct for improving such 4D datasets. In our laboratory, disk-scanning technology has largely replaced both CLSM and multi-photon microscopy for routine 4D data acquisition [Fig. 43.5(A–C)].

As an alternative to laser-based disk-scanning systems, other systems, such as the Atto CARV, use an arc lamp illumination source. When such systems are paired with sensitive EM-CCD cameras, they can often detect sufficient signal for studies on living embryos because, in this case, the fact that they send less excitation light to the specimen than the laser/micro-lens systems can be seen as an advantage [Fig. 43.5(D–F)].

Additional Hardware Improvements Can Increase Acquisition Speed

Additional improvements in the imaging system may also improve acquisition speed. An often-overlooked area in which significant gains have been made in recent years is in optical coatings and objective lens technology. Recent lenses from the major manufacturers have greatly improved transmission, and this has resulted in corresponding improvements in the ability to imaging very thin, small, dim structures in the light microscope.

A second potential improvement involves the use of piezoelectric focus controls, such as those on the PerkinElmer UltraView RS, which can move the objective lens rapidly and with little hysteresis in a step-wise fashion. Similar focus controls have been employed to move the objective continuously in the *z*-direction during a scan. Although this produces optical sections that are slightly tilted relative to the focal plane, one avoids the vibration and specimen movement that occurs when an immersion objective moves rapidly in a stepped manner (Hammond and Glick, 2000).

Finally, significant advances in camera technology allow for unprecedented speed of data collection. Back-thinned CCD cameras, such as those produced by Roper Scientific and Hamamatsu Corporation, and EM-CCD cameras, such as those produced by Andor Corporation (Chong *et al*., 2004), are having a profound influence on low-light microscopy. These cameras provide extremely fast readout with very low read noise and effective quantum efficiency, 2× to 3× higher than the best PMTs. EM-CCD technology in particular yields dramatic improvements in signal-to-noise ratio under ultra low-light conditions and high-speed operation. These cameras make it possible to capture low-read-noise images much more quickly for use in either deconvolution or disk-scanning confocal microscopy.

In the latter case, however, because the current generation EM-CCD cameras rely on frame transfer rather than interline transfer, the integrated charge pattern sweeps across the image field as it is being read out (i.e., the "electronic shutter" does not work so well, especially for short exposures). This creates a new source of artifact: if the position of the scanning disk is not synchronized with the CCD camera exposure and the vertical transfer axis of the CCD is not oriented properly with respect to the motion of the scanning disk, Moiré-type banding patterns are superimposed onto the image [Fig. 43.5(G–J)], particularly when one uses short exposure times. Although the time scale over which events in embryos occur is relatively long compared to the CCD exposure, this interference can nevertheless be a significant problem when attempting to minimize CCD exposure time during 4D acquisition.

Such "banding" can be greatly reduced or eliminated by carefully matching CCD frame transfer rates to the speed of Nipkow disk rotation. The newer CSU22 Yokagawa units permit variable speed disk rotation, which makes such matching easier (Chong *et al*., 2004). With some effort one can also match the fixed scan speed of the older CSU10 scan head, with the exposure times of at least some cameras, such as the iXon (Andor Corp., Belfast, UK). As this moiré problem is unrelated to the operation of the

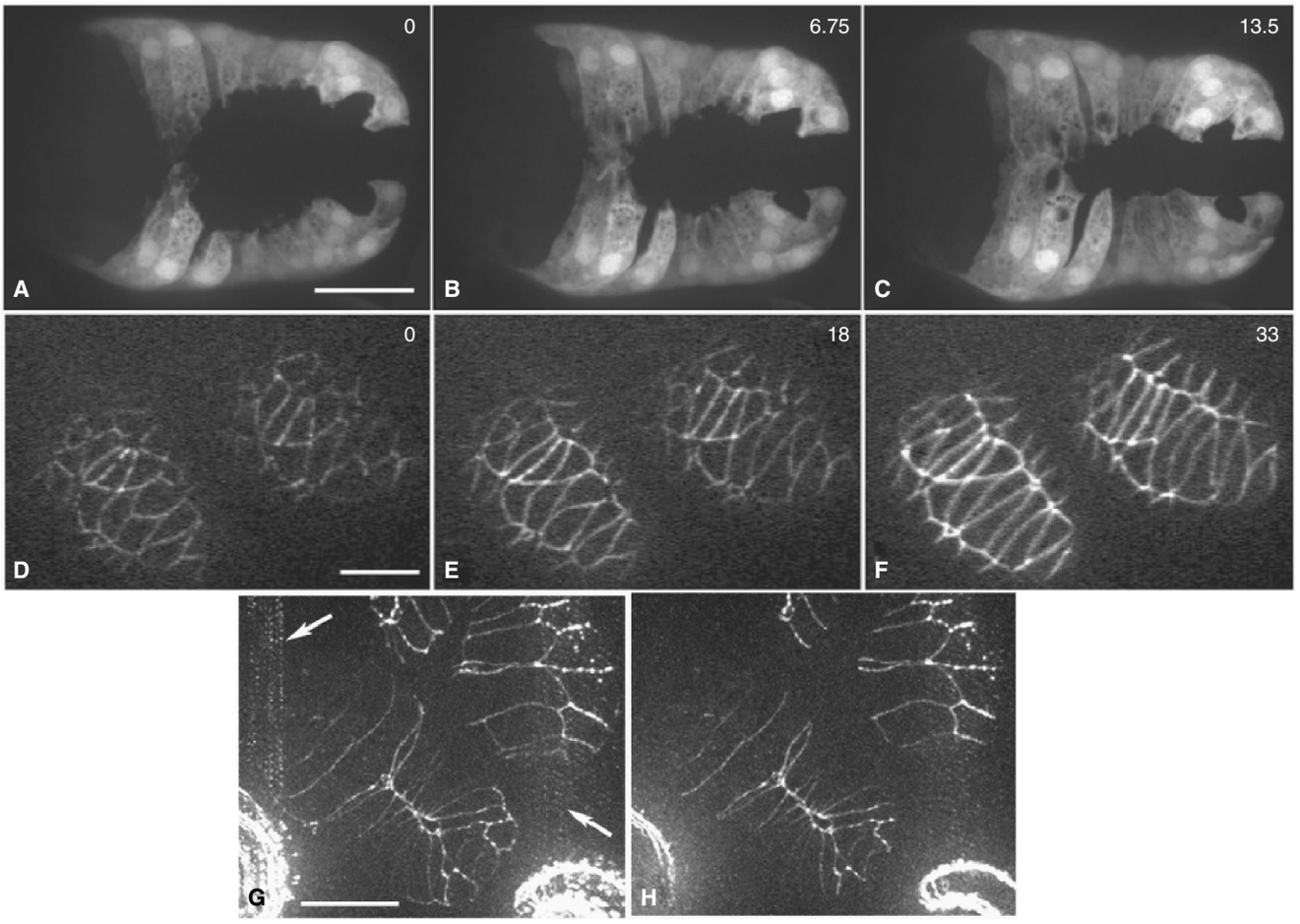

FIGURE 43.5. Disk-scanning microscopes can acquire 4D data quickly. (A–C) Frames from a 4D movie of ventral enclosure in a *C. elegans* embryo expressing a *dlg-1p : gfp* reporter acquired using a PerkinElmer UltraView LCI system equipped with a Hamamatsu Orca II ER CCD camera. Elapsed time in minutes is shown. *z*-stacks were acquired at 50 s intervals, 20 focal planes/stack; acquisition time/image, 300 ms. Fine details of protrusions are visible against a dark background using this particular transcriptional reporter. (D–F) Frames from a 4D movie of dorsal intercalation in a *C. elegans* embryo expressing AJM-1 : GFP, which localizes to epithelial junctions, acquired using an ATTO Carv system and a Roper Cascade B camera. *z*-stacks were acquired at 3 min intervals, 20 focal planes/stack; acquisition time/image, 700 ms. (G, H) A 30-focal-plane *z*-stack of images acquired using the system in (A), but imaged using an Andor iXon EM-CCD camera. Acquisition time/image 15 ms. Despite >30× shorter exposure time, junctional details are clearly visible. During acquisition, stop frame motion of maturing larvae was achieved for individual focal planes, despite their rapid muscle contractions (J. Hardin, data not shown). In (G), all 50 frames of the stack were projected using a maximum intensity procedure. Moiré banding is clearly visible (*arrow*). In (H), the top 30 frames were projected. No banding is visible, because the moiré pattern only became pronounced as the bottom half of the embryo was imaged. Bars = 10 µm.

electron multiplier, it will cease to exist when interline-transfer CCDs with EM readouts are introduced.

LOCALIZING LABEL: STRATEGIES FOR INCREASING EFFECTIVE CONTRAST IN THICK SPECIMENS

Methods for introducing fluorescent probes into living embryos vary from one model system to another. With the exception of fluorescent lipid dyes, fluorescent probes, including dyes and mRNA encoding various fluorescent proteins, are usually introduced into echinoderm, *Xenopus*, and zebrafish oocytes and embryos by microinjection. In other cases, fluorescent protein probes are introduced as transgenes, which are then expressed by the embryo as fluorescently tagged proteins. No matter what the method of introduction, there are several issues that must be addressed by developmental biologists as they use such probes. First, any probe can be susceptible to dominant-negative effects when used at high concentrations; fluorescent protein–tagged mRNAs or transgenes are no exception. Thus, developmental biologists must often balance the need for higher fluorophore concentration with such dominant-negative effects. Second, such effects appear to be system specific. Probes that work well in one system may be unacceptably toxic in another. As one of many examples, the lipid dye FM1-43, which has been used in several studies to label intracellular vesicles in living embryos (see below), causes toxicity to *Xenopus* oocytes, which are ordinarily fairly robust (Bement *et al*., 2003). Thus, as with most imaging experiments in living embryos, trial and error will be unavoidable. Third, in multi-channel experiments, the amounts of each labeled protein may need to be adjusted to avoid additive toxicity or artifactual effects. This issue is particularly important when the two proteins physically interact. Overexpression of such interactors can lead to large, artifactual aggregates within the cells expressing them (J. Hardin and C. Lockwood, unpublished observations).

Addition of Labeled Proteins to Embryos

Direct labeling of proteins or other probes is a tried and true method for introducing fluorescently labeled proteins into living embryos. This approach has worked particularly well for studying very early embryos or oocytes in amphibians (Bement *et al*., 2003) and echinoderms (Jaffe and Terasaki, 2004; Strickland *et al*., 2004). Although falling out of favor in deference to mRNA expression for production of transgenic embryos, direct labeling has the advantage that, unlike injection of mRNA or expression of fluorescently tagged transgenic constructs, there is no lag before expression is evident, and there are no complications involving efficient maternal expression of constructs. This virtue can also be a liability for studying events late in development: turnover of the labeled proteins may attenuate the concentration of labeled protein so severely by the stage of interest that it can be difficult to detect. However, this approach has worked well in some cases, including the study of embryonic neurons in amphibian embryos (Gomez and Spitzer, 1999). On the other hand, production and purification of fluorescently labeled proteins is typically much more difficult than injecting mRNA or making transgenics (at least in some organisms, such as *C. elegans* or *Drosophila*). Moreover, directly conjugated fluorescent proteins must typically be centrifuged at high speed to remove unconjugated label (e.g., 100,000 g). Several companies make prelabeled proteins for study of the cytoskeleton that ameliorate these difficulties, including fluorescently labeled phalloidin and taxol for labeling F-actin, as well as cytoskeletal monomers labeled with fluorophores (Bement *et al*., 2003).

Expressing Green Fluorescent Protein and mRFP Constructs in Embryos Allows Dynamic Analysis of Embryos at Multiple Wavelengths

The discovery and widespread use of GFP as a tag for visualizing gene expression and protein localization within living organisms has revolutionized live embryo imaging (Chalfie *et al*., 1994). GFP (especially the widely used multiply-mutated version known as EGFP) is bright, generally non-toxic, and resistant to photobleaching. The advent of numerous color shifted spectral variants of GFP (Miyawaki *et al*., 2003), including enhanced cyan and yellow fluorescent proteins (ECFP and EYFP, respectively) has allowed multiple fluorescent proteins to be detected simultaneously in living embryos (Hadjantonakis *et al*., 2003), and has made possible techniques such as *in vivo* FRET (see below). Recent identification of a red fluorescent protein from coral (DsRed) allows the fluorescent-protein approach to be extended deep into the red portion of the visible spectrum. Although earlier versions of DsRed were multimeric and hence slow to assemble into a functional fluorophore, multiple mutations have now resulted in a monomeric form of the protein, mRFP1 (Campbell *et al*., 2002), that folds much more rapidly and hence serves as a suitable FP for dynamic events in early embryos. The recent advent of color-shifted variants of DsRed (Shaner *et al*., 2004) will make this family of fluorophores even more useful. We (see Fig. 43.7) and others (Benink and Bement, 2005) have begun using mRFP1 along with EGFP to perform dual-channel imaging of fluorescence, indicating that fluorescent proteins will continue to be the method of choice in genetic systems in which fluorescent-protein-tagged transgenes can be introduced. Ways of introducing fluorescent-protein-tagged constructs into embryos involve system-specific techniques beyond the scope of this chapter; here we make several generalizations about the uses of various strategies for imaging embryos expressing fluorescent-protein-tagged constructs.

Transcriptional Reporters Allow Analysis of Dynamic Processes in Embryos

To developmental biologists, fusing the coding region of EGFP to the regulatory DNA associated with a gene of interest (i.e., GFP reporter constructs) is often used to assess the tissue-specific and temporal patterns of the transcriptional activation of a gene. Such data provides valuable information about how the expression of a gene is regulated. However, such transcriptional reporters can also be invaluable for live embryo imaging for several reasons. First, such reporter constructs result in the expression of GFP in the cytosol; because GFP is fairly small, these reporters are capable of percolating into small volumes within the cytoplasm, including the fine protrusions extended by cells as they migrate (Fig. 43.6). Second, the highly specific expression pattern of some genes allows either many or a very small number of cells to be visualized against a dark background, dramatically improving the effective contrast of the specimen being imaged. In some cases, such effective contrast enhancement can be aided by dual labeling with more general fluorescent counterstains (see below). Third, imaging cytosolic GFP reporters typically does not cause as much photodamage as with GFP translational fusions. Thus, in some cases where a membrane-localized GFP or similar translational fusion construct might be desirable, a cytosolic GFP may be sufficient for tracking cell trajectories or monitoring protrusive activity.

Translational Fusions Allow Analysis of the Subcellular Distribution of Specific Proteins

Using molecular techniques to fuse fluorescent proteins to a peptide or protein sequence has transformed cell and developmental biology by allowing the *in vivo* analysis of intracellular protein dynamics (Lippincott-Schwartz and Patterson, 2003). In addition, however, fluorescent-protein-labeled proteins can serve the developmental biologist by allowing the analysis of cell and tissue movement in 4D. For live embryo work, several such translational fusions are generally useful. Fluorescent-protein-tagged nuclear proteins, such as histone H2B (Megason and Fraser, 2003) can be an effective means by which to track cell positions, in addition to their obvious use in studying nuclear dynamics in embryos. As an indirect readout of cell position without the complexities of fluorescent cell borders, tracking of nuclei can be a useful tool for charting overall cell movements. Cell membrane localized fusions, such as fusions to the GAP-43 membrane-localization signal or the Lck membrane-localization signal to drive membrane localization (Megason and Fraser, 2003) can be used to outline cell membranes. For studying morphogenetic movements in embryos, junction-localized fluorescent proteins are extremely useful. Our laboratory has used junction-localized fluorescent proteins to study epithelial sheet movement in *C. elegans* (Mohler *et al*., 1998; Köppen *et al*., 2001). Others have used moesin :: GFP to analyze *Drosophila* morphogenesis in a similar manner (Edwards *et al*., 1997). Three examples of dual labeling with EGFP and mRFP1 fusions are shown in Figure 43.7.

Translational fusions can, of course, be coupled to highly tissue-specific promoters to yield probes that are both subcellularly localized and expressed in a restricted group of cells. As one example among many, this approach has been used to visualize actin-based protrusions in leading edge cells during dorsal closure in *Drosophila* by driving expression of constructs using the engrailed promoter, which yields well-defined stripes of expression (Jacinto *et al*., 2000).

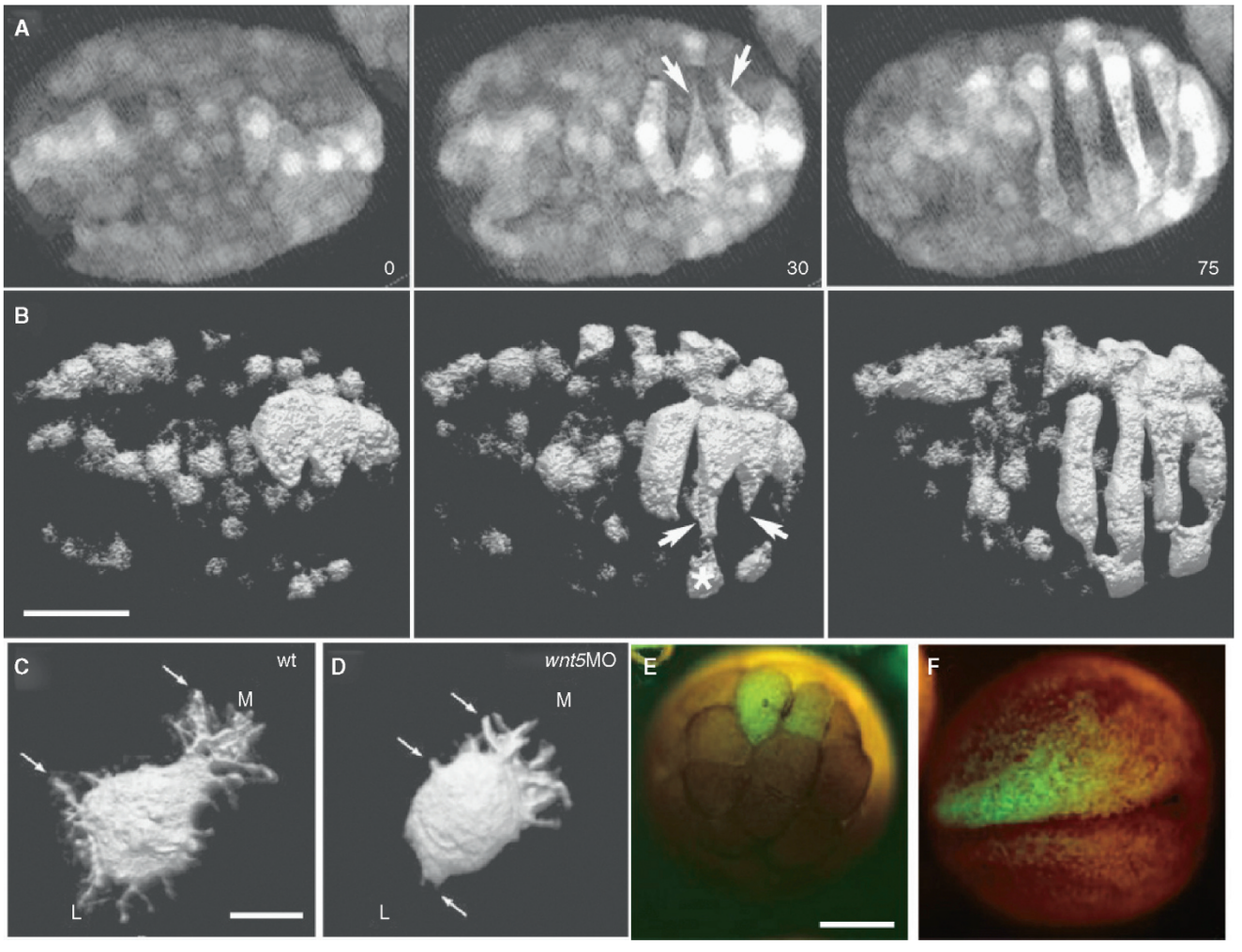

FIGURE 43.6. Cytosolic markers allow imaging of cell motility and cell movement in embryos. (A, B) Frames from 4D movies of dorsal intercalation in *C. elegans* embryos expressing *lbp-1p::gfp*, which is expressed in a subset of dorsal epidermal cells. (A) An embryo imaged using MPLSM (Heid *et al*., 2001) using a Ti:Sa laser and descanning through a Bio-Rad 1024 scanhead. *z*-stacks were subsequently 3D projected using a maximum brightness procedure. (B) A similar embryo imaged using the disk-scanning apparatus described in Figure 43.5(A). The dataset in (B) was subsequently subjected to surface rendering using Volocity software. Fine protrusions are visible in both cases. In (B), it is clear that the protrusions are wedge-shaped in the *z*-dimension, and that the non-dorsal cell (*asterisk*) also produces fine protrusions. Bar = 10 µm. (C, D) Protrusive activity of zebrafish mesodermal cells imaged in wild-type (C) and Wnt5a morpholino injected embryos (D) expressing a combination of cell surface (GAP43::GFP) and cytosolic GFP. Images were acquired using a Bio-Rad Radiance 2000 MPLSM equipped with a Ti:Sa laser; three successive stacks of 120 focal planes each were acquired, one of which is shown here. The resulting images were surface rendered using Volocity software. These cells display oriented protrusive activity. The cell from the morpholino injected embryo displays impaired motility. Bar = 10 µm. (E, F) Quantum dot (QD) labeling of cells in an early *Xenopus* embryo. QD micelles were injected into an individual blastomere during very early cleavage stages. Between 1.5 and 3 nL of a 2.3 µ*M* suspension of QDs were injected, corresponding to 2.1 to 4.2×10^9 injected particles per cell. (E) Injection of one cell in an eight-cell-stage embryo resulted in labeling of individual blastomeres. (F) The daughter cells of the injected blastomere are labeled at the neurula stage. Embryos were imaged with Chroma filter set 41015 (wild-type GFP longpass emission with a 50 nm wide bandpass excitation centered at 450 nm) mounted on a Zeiss fluorescence microscope. Bar = 500 µm. [(A) is from Heid and colleagues (2001); (B) is courtesy R. King and T. Walston, University of Wisconsin; (C, D) are from Kilian and colleagues (2003); (E, F) are from Dubertret and colleagues (2002), used by permission.]

Using Selective Labeling to Reduce the Number of Labeled Structures

Dextran Labeling

Injecting fluorescent dextrans into the blastomeres of early embryos has a long history in developmental biology (e.g., Gimlich, 1991). Focal injections allow the progeny of injected cells to be visualized against an unlabeled background during later development, a process that permits one to develop fate maps. Live 4D imaging using confocal or multi-photon microscopes allows the progeny of such injected cells to be followed with remarkable clarity. For example, the cells shown in Figure 43.10(D–F) are the progeny of blastomeres of a zebrafish embryo injected early in development, and have been imaged at high resolution and followed in 4D space.

Quantum Dots

Fluorescent semiconductor nanocrystals, or quantum dots (QDs), have the potential to be useful for long-term observations via confocal and (especially) multi-photon microscopy as an alternative

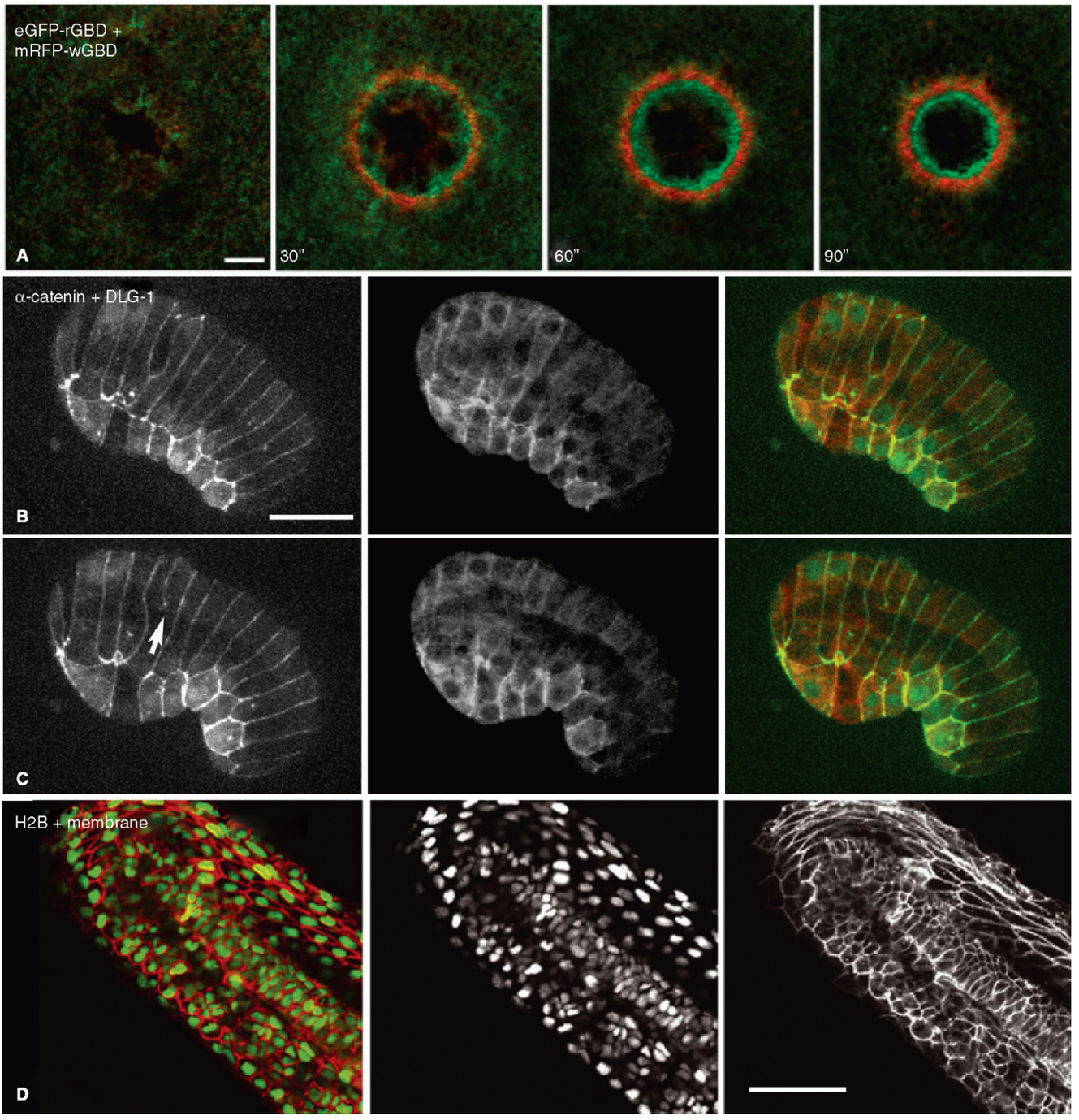

FIGURE 43.7. Simultaneous imaging of GFP- and mRFP-tagged proteins in living oocytes and embryos. Three different examples of using dual-channel imaging to detect GFP- and mRFP translational fusions. (A) Frames from a movie showing that RhoA (detected using eGFP-rGBD; green) and Cdc42 (detected using a fusion between mRFP and a protein fragment that binds active Cdc42; red) segregate into discrete zones during wound healing in a *Xenopus* oocyte (time in seconds). Imaging was performed as in Figure 43.1(A). Bar = 10 µm. (B, C) Frames from a movie of elongation of a *C. elegans* embryo expressing DLG-1 :: mRFP and HMP-1/α-catenin :: GFP (left) DLG-1 :: mRFP; (middle) HMP-1 :: GFP (right, overlay). Loss of junctional material occurs at sites where epidermal cells are fusing (*arrow*). (B, C) are 75 min apart. Imaging was performed as in Figure 43.6(A). Bar = 10 µm. (D) Dorsal–lateral view of the tail of 24 h living zebrafish embryo injected with RNA for Histone H2B–EGFP and membrane-localized mRFP1. (Left) Both channels together. (Center) Histone H2B–EGFP channel. (Right) Membrane mRFP1 channel. The nuclei can be discerned even in areas where they are closely packed such as the spinal cord (running along middle of the tail). Bar = 100 µm. [(A) is from Benink and Bement (2005); (B, C) are courtesy C. Lockwood, University of Wisconsin; (D) is from Megason and Fraser (2003), used by permission.]

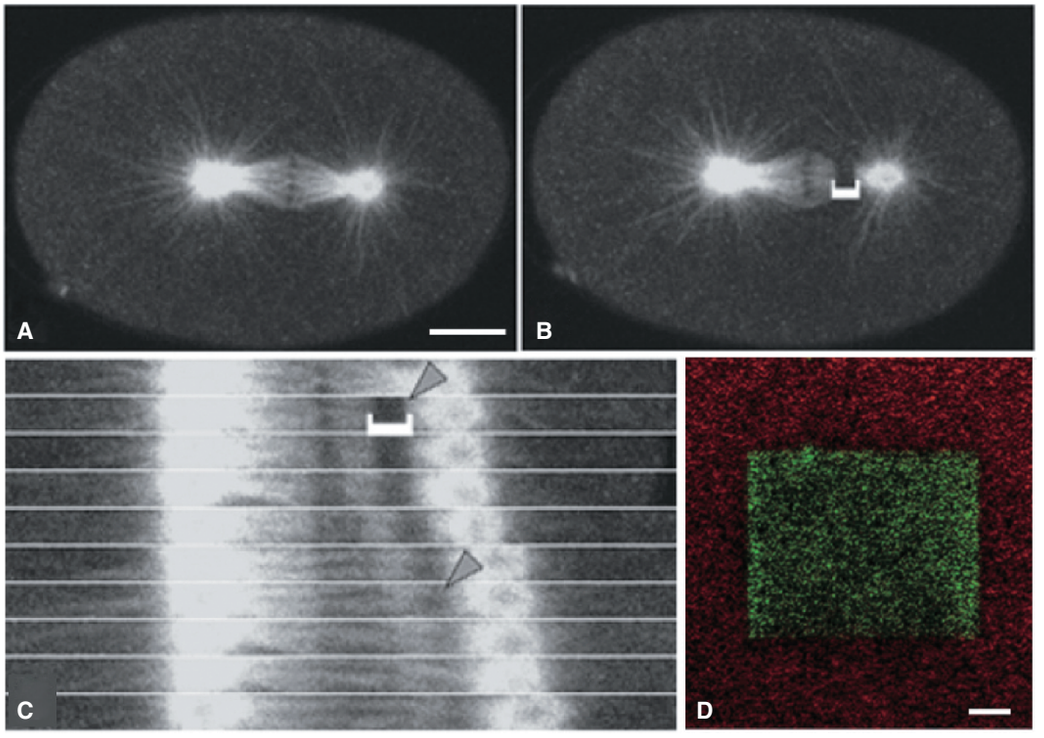

FIGURE 43.8. Using fluorescence recovery after photobleaching (FRAP) and photoactivatiable GFP in embryos. (A–C) FRAP of GFP-tagged microtubules in a living *C. elegans* zygote. Time-lapse images of embryo expressing β-tubulin::GFP (A) in which a short region of the posterior spindle microtubules was photobleached during anaphase onset (B, *bracket*). The kymograph below (C) follows the movement of the photobleached region (indicated by *gray arrowheads*). Frames were acquired at 7 s intervals using a Zeiss LSM 510 LCSM. For photobleaching, a selected region of interest was photobleached using 50 to 150 1s scans of 100% 488 nm laser power. Bar = 10 µm. (D) Photoactivation of PA-GFP at the surface of a *Xenopus* oocyte using a LCSM. A *Xenopus* oocyte injected with mRNA encoding mRFP- (red) and PA-GFP tagged forms of a synthetic F-actin binding peptide was scanned repeatedly with the 488 nm line from a Bio-Rad 1024 LCSM to photoactivate PA-GFP. Bar = 10 µm. [(A–C) are from Labbe and colleagues (2004); (D) is courtesy of B. Burkel and W. Bement, University of Wisconsin.]

to fluorescent dextrans for lineage tracing. Compared with organic dyes and fluorescent proteins, QDs offer several advantages (Gao *et al*., 2005; Michalet *et al*., 2005). First, the manufacturing process yields QDs with highly specific composition- and size-dependent emission characteristics that are tunable throughout essentially the entire visible and NIR spectrum, all excitable by a single wavelength. Second, QDs have a very high absorption cross-section. As a result, a very small number of QDs are necessary to achieve a detectable signal; in some cases it has been possible to detect the fluorescence of single or small numbers of QDs. Third, QDs have a large Stokes shift, which may be an advantage in situations where autofluorescence of the tissue would mask the emission signal of fluorescent dyes. Finally, the high electron density of QDs allows them to be viewed via TEM, making them useful for correlative studies (see Chapter 49, *this volume*).

Although QDs have been used without derivatization, typically they are encapsulated in a polymer shell. Dubertret and colleagues encapsulated QDs within PEG-derivatized phospholipid micelles, and injected them into early blastomeres in *Xenopus* embryos (Dubertret *et al*., 2002). They found that the QDs were extremely stable, and when injected at sufficiently low concentrations caused no toxicity [Fig. 43.6(E,F)]. Although this technology is still emerging, QDs have tremendous promise in the future for use in living embryos under prolonged observation.

Photobleaching

GFP can be used very successfully in studies involving fluorescence recovery after photobleaching (FRAP) and related technologies (Lippincott-Schwartz *et al*., 2003), which is easily done via repeated scanning of a selected area in the LSCM. Although in some cases, it is likely that photobleaching will result in unacceptable photodamage (see Chapter 49, *this volume*), it has been used successfully in several experiments with live embryos (e.g., Benink *et al*., 2000; Labbe *et al*., 2004) [Fig. 43.8(A–C)].

Photo-Activatable Dyes and Photo-Activable GFP

Another technique for marking small groups of cells involves the use of photo-activatable, or caged, fluorophores. Such fluorophores only fluoresce after the caging group is removed by photocleavage at the appropriate wavelength, typically in the violet or near ultraviolet (UV). Caged fluorescein dextran has been used for fate mapping in both *Drosophila* (Girdham and O'Farrell, 1994) and zebrafish (Kozlowski *et al*., 1997). Although widefield imaging was used to track the resulting fluorescein fluorescence, confocal and multi-photon imaging are also well-suited to this approach.

More recently, a photoactivatable variant of GFP (PA-GFP) was described (Patterson and Lippincott-Schwartz, 2002). PA-GFP

only fluoresces after photo-activation via intense irradiation with 413 nm laser light, or by exposure to a standard mercury arc. The fluorescence of PA-GFP has been reported to increase at least 60× after activation *in vivo*. Once activated, it appears to be as stable as other GFP variants (Patterson and Lippincott-Schwartz, 2002). Recently, PA-GFP was used to follow local movements of, and recruitment of actin in, wounded *Xenopus* oocytes [Fig. 43.8(D)]; in this case, PA-GFP was photoactivated by a brief pulse of laser light from the standard 488 nm line of a Bio-Rad 1024 CLSM, indicating that all steps, from photo-activation to imaging, can be performed using 4D CLSM (B. Burkel and W. Bement, personal communication). The use of PA-GFP in the live imaging of embryos will undoubtedly become more widespread in the immediate future.

An alternative to PA-GFP is the use of kindling proteins (Chudakov *et al*., 2003). This approach relies on a chromoprotein, asCP, isolated from the sea anemone *Anemonia sulcata*. asCP is not fluorescent until it is irradiated , or kindled, using intense green light; kindled asCP then emits at 595 nm. A mutant form of asCP (KFP1) has been produced that undergoes irreversible kindling when irradiated with intense green light (e.g., brief irradiation at 30% power using a 543 nm laser on a Zeiss LSM 510 CLSM), but can be reversibly kindled when irradiated at lower power (e.g., 5% power on the same apparatus). Reversibly kindled KFP1 can be quenched by irradiation with blue light (using the 458 nm line of the same device at 1% power). Like original forms of DsRed, KFP1 currently requires multimerization for function. If a monomeric form of KFP1 can be produced, it may have properties which will be more generally useful for imaging living embryos beyond current applications, which only involve fate mapping (Chudakov *et al*., 2003).

Directly Conjugated Antibodies for Visualizing the Extracellular Matrix

Although extracellular matrix (ECM) components have been successfully visualized by making GFP-tagged translational fusions, another approach for localized labeling of the ECM is the injection of antibodies specific for particular components directly conjugated to fluorophore. This approach has been used successfully to visualize fibrillin in the chick embryo (Czirok *et al*., 2004), and fibronectin in *Xenopus* embryos (L. Davidson, R. Keller, and D. Desimone, personal communication). Using this approach, labeled fibrils can be imaged for long periods of time to track their movement during morphogenesis (Czirok *et al*., 2004).

Bulk Vital Labeling Can Enhance Contrast

While the use of GFP, mRFP1, and their spectral variants has led to huge advances in our ability to image embryos, these approaches have some limitations. First, producing DNA constructs for expressing GFP-tagged versions of proteins within embryos requires multiple cloning steps, some of which can be arduous, especially for large genes. Second, when introduced as mRNA or as transgenes, these proteins are often over-expressed, and care must be taken so that over-expression artifacts do not compromise the final results. Third, it is often difficult to target GFP- or mRFP-tagged constructs to a broad spectrum of subcellular compartments, although there are several recent examples in which GFP has been targeted to membranous organelles (Poteryaev *et al*., 2005). Finally, in organisms such as *C. elegans*, it is difficult to introduce mRNAs by direct injection. This can make it hard to achieve high levels of expression in the germline, with the result that exogenous promoters must sometimes be used to generate enough expression to visualize the protein of interest in the early embryo (Strome *et al*., 2001).

One solution to these problems is to use fluorescent vital dyes. Such dyes have the virtue that they can label many cells in the embryo simultaneously, partitioning preferentially into specific cellular structures based on their chemical properties. Several dyes have proven useful for this purpose:

1. **Unconjugated BODIPY and BODIPY-ceramide dyes**: "BODIPY" is a trade name for a class of photostable, neutrally charged, boron-containing diazaindacene fluorophores that span much of the visible spectrum (Molecular Probes, 2004). Several unconjugated BODIPY fluorophores, such as BODIPY 505/515, have been used as vital fluorescent stains for zebrafish embryos, where they localize to intracellular yolk platelets and in intercellular spaces. BODIPY-ceramide has been used to label the plasma membrane and endomembranes [Fig. 43.9(A–C)]. Embryos can be bathed in these dyes, allowing most cells in the embryo to be stained rapidly (Cooper *et al*., 1999).

2. **FM4-64, FM1-43, and other lipophilic membrane dyes**: FM4-64 is a red fluorescent membrane dye that is useful for outlining plasma membranes. Such lipophilic dyes work well for bulk labeling of plasma membranes in a variety of species. Like DiI, multi-photon imaging of FM4-64 requires the use of a Nd:YLF laser. Using such technology, dynamic membrane-associated events have been followed during *C. elegans* development using 4D imaging (Mohler *et al*., 1998) [Fig. 43.9(D)]. An alternative is FM1-43, a water-soluble, styrylpyridinium dye that more generally labels membranous structures, likely by inserting into the outer leaflet of the plasma membrane, where it becomes highly fluorescent. FM1-43 has been used to study exocytosis during echinoderm fertilization (Terasaki and Jaffe, 2004) and to study vesicular trafficking in early *C. elegans* embryos (Skop *et al*., 2001) [Fig. 43.9(E)].

3. **DiI derivatives**: The lipophilic carbocyanines DiI [DiIC18(3)], DiO [DiOC18(3)], DiD [DiIC18(5)], and DiR [DiIC18(7)], are weakly fluorescent in water but highly fluorescent and very photostable when incorporated into membranes. DiI, DiO, DiD, and DiR exhibit distinct orange, green, red, and infrared fluorescence, respectively, thus facilitating multi-color imaging (Molecular Probes, 2004). By varying the number of carbons attached to the fluorophore, the hydrophobicity of the dye can be varied. The slightly less lipophilic DiIC12(3), DiIC16(3), and DiOC16(3) are sometimes easier to dissolve and load into membranes than their C18 homologs (Molecular Probes, 2004), but can also yield more non-specific labeling than their longer-chain counterparts (J. Hardin, unpublished observations). Longer carbon chains result in poor solubility, even in the presence of a carrier such as DMSO. The result is that, in saline media or seawater, the dye forms tiny crystals. Cellular structures are only labeled when a crystal physically touches a membranous structure. In the case of sea urchin embryos, for example, incubation of embryos with DiC_{16} for 5 min results in a salt-and-pepper pattern of cell labeling that allows individual cells to be followed against a dark background. Multi-photon imaging of labeled cells is possible using a Nd:YLF laser operating at 1047 nm [Fig. 43.9(F,G)].

4. **BODIPY TR, methyl ester dye**: BODIPY TR, methyl ester dye, readily crosses cell membranes and localizes to membrane-bound organelles. Because the dye does not localize strongly to the plasma membrane, BODIPY TR, methyl ester is useful for determining the position of the nucleus and the shapes of cells, and for outlining whole tissues. The emission maximum

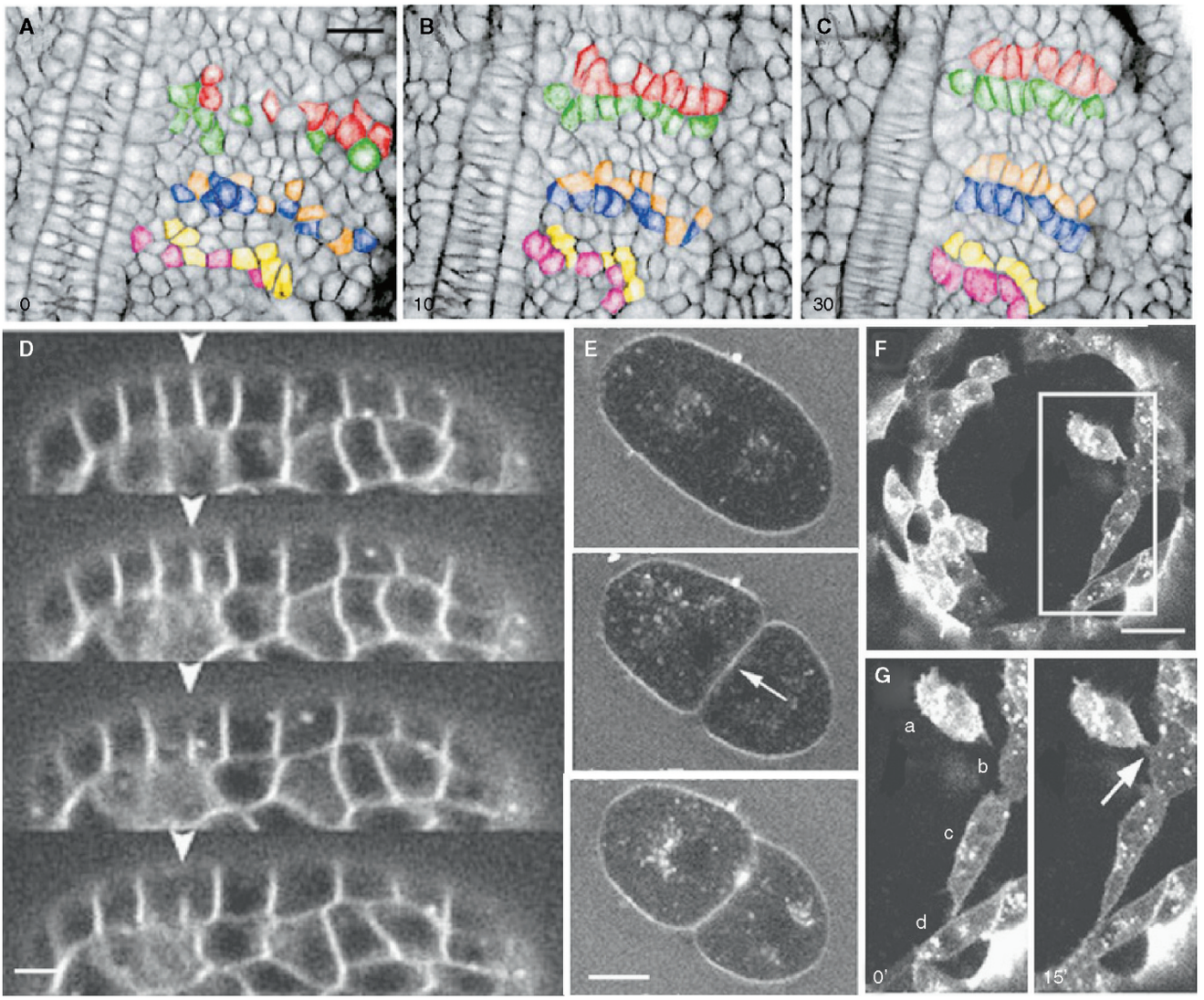

FIGURE 43.9. Bulk labeling with dyes in living embryos. Four different examples of the use of bulk-dye labeling in living embryos. (A–C) Time-lapse sequence showing somitogenesis in a one-somite stage zebrafish embryo (dorsal view, anterior at top). Embryos were vitally stained with the fluorescent lipid Bodipy-C5 ceramide and observed using a Bio-Rad MRC-600 CLSM. The elapsed time (min) is indicated in each panel. Individual somitic cells are colorized for clarity. As somites form, intercalation of cells forces colorized and non-colorized cells to rearrange, changing the overall shape of the tissue. Bar = 20 µm. (D) Live MPLSM imaging of epidermal cell fusions in the *C. elegans* embryo. Frames are 5.5 min apart. Disappearance of lateral membranes (*arrowhead*) in an optical cross-section of an embryo labeled with FM4-64 indicates cell–cell fusion is occurring. Images were acquired using a 1047 nm Nd : YLF laser and a Bio-Rad MRC-600 scan head with no pinhole inserted in the optical path. Bar = 5 µm. (E) Plasma membrane dynamics in the early *C. elegans* embryo studied using FM1-43. MPLSM time course of a single focal plane taken from an embryo labeled with FM1-43 during cytokinesis. Elapsed time is shown in minutes. Cytokinetic furrow formation completed at 3.0 min. Membrane accumulates at a specific focal spot (*arrow*, 4 min), and continues to accumulate in successive time points. Bar = 10 µm. (F–G) Cell rearrangement at the blastopore of a sea urchin embryo visualized using $DiIC_{16}$. (F) Blastopore view of a $DiIC_{16}$ normal late-gastrula embryo. The dark area in the center is the blastopore surrounded by $DiIC_{16}$-labeled cells at the blastopore lip; the inset is enlarged in (G, H). (G, H) Frames acquired 15 min apart showing movements of cells. Cell **a** has produced a protrusion (*arrow*) and made contact with cell **b**, while cells **c** and **d** have shifted positions. Bar = 10 µm. [(A–C) are from Henry and colleagues (2000); (D) is from Mohler and colleagues (1998), used by permission.]

of BODIPY TR, methyl ester is at ~625 nm, making it an excellent counterstain for eGFP (emission maximum ~508 nm; Cooper *et al*., 2005), one that produces little spectral bleed-through of GFP fluorescence into the BODIPY TR channel. The excitation curves of the two fluorophores are well separated as well, making them suitable for dual-channel confocal imaging [Fig. 43.10(A–C)].

5. **Scatter labeling using lineage tracers**: When injected into blastomeres that generate a large sector of the embryo, lineage tracers, such as fluorescent dextrans, can serve as an effective counterstain. This technique has been used effectively in zebrafish embryos [Fig. 43.10(D–G)].

SEEING IN SPACE: STRATEGIES FOR 4D VISUALIZATION

To one accustomed to normal, 2D, widefield fluorescent microscopy, the images presented by any of the 3D microscopy methods mentioned above can seem such an improvement that many are tempted simply to page through the planar images, feeling perhaps that the time spent to make a proper 3D or 4D rendering would be better spent obtaining more data. However, this temptation should be avoided, because 3D reconstructions provide wonderful new perceptual insights into embryogenesis.

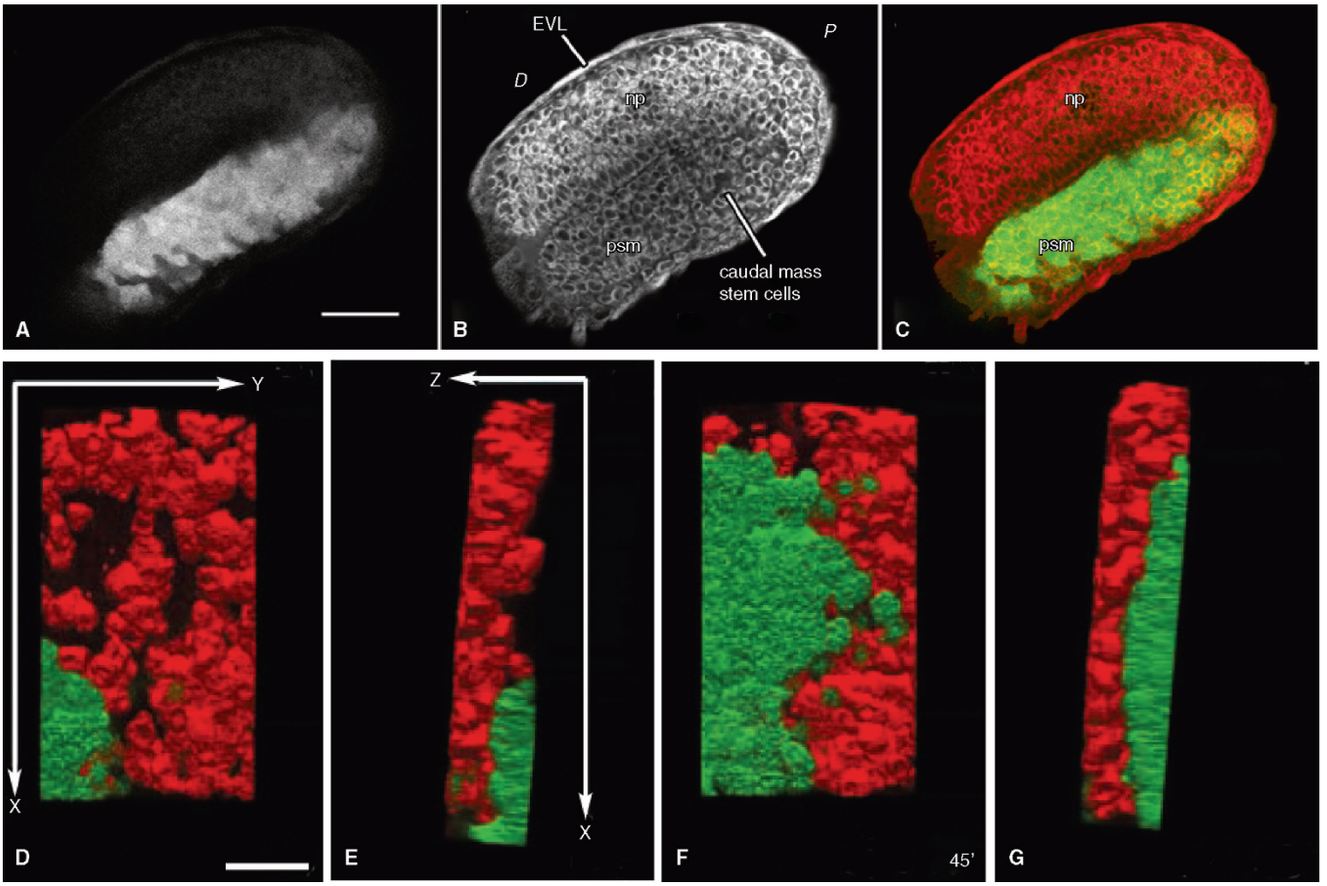

FIGURE 43.10. Counterstains can improve visualization of GFP-expressing cells in embryos. (A–C) BODIPY TR methyl ester counterstaining in a living zebrafish embryo, imaged using a Bio-Rad MRC-600 CLSM. (A) Tail rudiment of a tbx6-GFP transgenic, 19-somite embryo (lateral view). GFP is expressed in the caudal mass stem cells. D, dorsal; P, posterior. (B) BODIPY TR methyl ester dye fluorescence. Loosely organized mesenchymal stem cells join cells in the posterior limit of the presomitic mesoderm (psm). Np, neural plate. (C) Merge. Scale bar = 100 µm. (D–G) Counterstaining using fluorescent dextran. Zebrafish embryos expressing GFP (green) under the control of the goosecoid (gsc) promoter in prechordal plate precursor cells were scatter-labeled with rhodamine (red) in epiblast cells overlying the presumptive prechordal plate and followed in 3D over time by dual-channel confocal microscopy using a Bio-Rad Radiance 2000 CLSM. Surface renderings were performed using Volocity software. gscGFP embryos at shield stage (D, E; E is a rotated view of D) and 45 min later (F, G). In all pictures, anterior is to the top and posterior to the bottom. Bar = 50 µm. [A–C are from Cooper *et al.* (2005); D–G are from Ulrich *et al.* (2003). Used by permission.]

One of the challenges of 4D live imaging of embryos is visualizing the resulting datasets in meaningful ways. Although these challenges are not unique to embryos, the widespread use of 4D imaging in developmental biology requires efficient ways to navigate through 4D datasets, to project or render them as 2D + time or 3D + time datasets, and to provide compiled datasets to other researchers in a portable, compact format.[5] As an example, consider the embryo in Figure 43.11, which expresses a GFP-tagged protein that localizes to epithelial junctions, and has been imaged using two-photon microscopy (Köppen *et al.*, 2001). Images acquired at different focal depths provide simultaneous information about structures throughout the thickness of the embryo [Fig. 43.11(A,B)], but without any sort of projection or reconstruction, it is difficult for the typical student or researcher to mentally manipulate information from each of the focal planes simultaneously.

Depicting Embryos in Time and Space: 2D + Time Versus 3D + Time

While 4D confocal datasets can yield powerful views of single focal planes in embryos over time, examination of such datasets immediately presents a challenge: single optical planes contain a limited amount of spatial information along the imaging axis. Thus, a key challenge in 4D confocal imaging of embryos is navigating through the raw 4D dataset quickly and easily (i.e., up and down within a single time point, and a single plane across time points). The challenge extends beyond navigation through the raw

[5] Older, platform-specific software solutions for compiling and browsing 4D datasets have been described (Mohler, 1999). More recently, several platform-independent solutions have emerged; several make use of the extensible plug-in architecture of ImageJ (http://rsb.info.nih.gov/ij/). These include the HyperVolume Browser plug-in by P. Pirrotte and J. Mutterer (http://rsb.info.nih.gov/ij/plugins/hypervolume-browser.html), which allows a folder of images collected as a 4D dataset to be played back within RAM. A solution that is much less RAM-intensive is to compile 4D datasets into QuickTime movies; such movies have the tremendous advantage that they are portable, and can be played back on rather unremarkable computer hardware. I have written a Java-based software suite that fulfills this purpose within ImageJ, including a browser to preview 4D datasets before compression (Browse4D), a compressor (QT4D Writer), and a viewer (QT4D Player). The suite is available for download at http://worms.zoology.wisc.edu/QT4D.html.

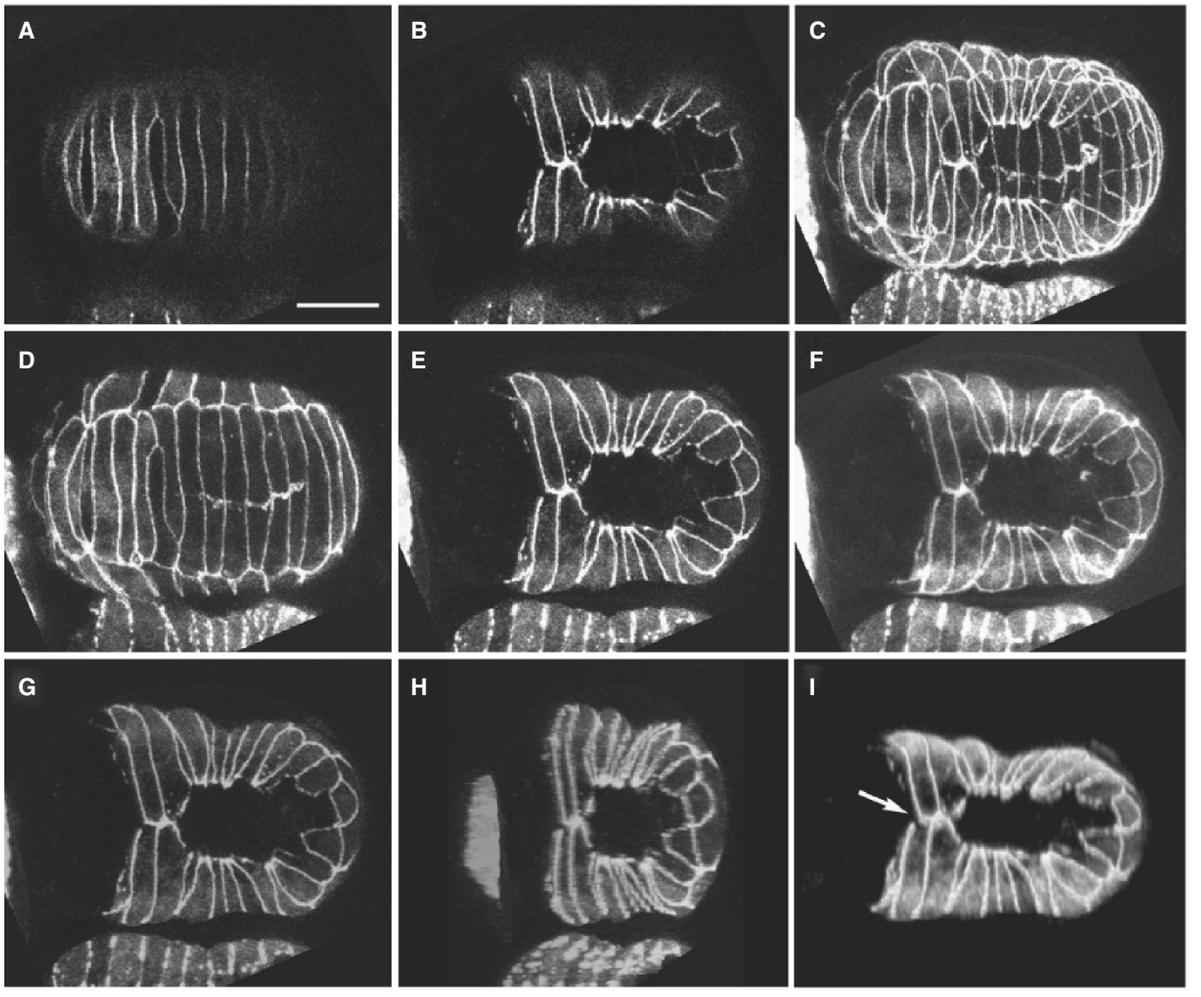

FIGURE 43.11. Using projections can simplify viewing of three-dimensional embryos. (A) Single *C. elegans* embryo expressing DLG-1:GFP (a protein that localizes to epithelial junctions) imaged using MPLSM. Thirty focal planes spaced at 1 µm were acquired. (A) A focal plane deep within the specimen (focal plane 27), showing the dorsal epidermis. (B) A focal plane near the coverslip (focal plane 5), showing the ventral epidermis from the same embryo. (C) A maximum intensity, 2D projection of all 30 focal planes allows visualization of most structures, but material from the ventral surface obscures dorsal structures. (D) A maximum intensity, 2D projection of focal planes 17 to 29, effectively visualizing dorsal structures. (E) A corresponding ventral-only projection (focal planes 3–10). (F) Focal planes 3 to 10 projected using an average intensity projection, followed by contrast enhancement. (G) A 3D projection of focal planes 3 to 10 performed using ImageJ, using the brightest point method, with 0° of rotation. (H) Same data set rotated 50° around the *y*-axis. I. Same dataset visualized as a voxel-based projection using Volocity. The arrows point to the ventral midline, where it is clear that epidermal cells lay down a midline septum of some thickness. Bar = 10 µm.

4D datasets, however. To image the entire embryo or a spatial subset of the 4D dataset, the embryo must be rendered at each time point in such a way that information from multiple focal planes is displayed over time.

There are two common strategies for displaying typical 4D datasets. The multiple optical sections from an image stack can be projected along the *z*-axis to form a 2D dataset, thereby flattening the 3D data (2D + time). Alternatively, the voxels of each original 3D volume can be rendered using a number of different algorithms (3D + time) and then these renderings can be linked to form a movie. In the 2D + time approach, the 3D spatial information in the specimen is lost, but the predominant features of the 3D volume are represented in a format that is computationally less demanding. 2D + time strategies are particularly effective for displaying information from a volume that is relatively thin along the *z*-axis [Fig. 43.11(D–F)]. If most cellular movement occurs in a plane or within a few optical sections, this approach is often the best for qualitative visualization of important details in the dataset.

Some software packages, such as the UltraView software provided with PerkinElmer disk-scanning microscopes, allow adjustable selection of a specific subset of focal planes for projection over time. This provides an animated movie of the equivalent of a thick optical slab over a specific range of *z*-positions within the dataset, but with an important difference: unlike an actual optical thick section, particular features within the slab are still seen distinctly. Many other software packages, including ImageJ, allow projection of single *z*-series, and permit the writing of plug-ins or macros that provide semi-automated production of projected 2D + time datasets.

Various algorithms can be used to project a stack of optical sections (see Chapters 14 and 15, *this volume*). Developmental biologists typically wish to view the readout of the prominent fluorescent details within a volume more directly. To do this, two

sorts of projection strategies are employed: maximum-intensity and average-intensity projections. The maximum-intensity algorithm queries the intensity of a pixel (or neighborhood of pixels) at a given *x*,*y*-position in the projected image, and selects the brightest pixel for display at that position along the line of projection within the image stack.

Maximum-intensity projections [Fig. 43.11(C–E)] are typically the favorite of developmental biologists, because they emphasize the brightest details in the volume, and these are often the most interesting (see Chapter 14, *this volume*). One weakness of maximum-intensity projections is that they are susceptible to artifacts from noise in individual optical sections within the stack. We have found that in such cases, applying standard Gaussian filters can significantly improve the starting image. In general, however, the best projections begin with images that have high intrinsic signals. Another drawback of maximum-intensity projections is that, because they deliberately emphasize small but bright fluorescent structures, they are not really suitable for quantification and they also tend to make near features obscure other features inside the data volume.

The average-intensity projection algorithm sums all of the pixel intensity values along a projection through the stack, calculates the average pixel value, and displays that value at the corresponding position in the projected image. Average intensity projections are less noisy, and are typically considered to produce a more quantitatively accurate representation of the data. Because calculating an average along a projection line that contains many zero intensity pixels reduces the visible contrast of such projections, the results should be viewed using a high contrast look-up table to yield results that are similar to those of maximum intensity projections [Fig. 43.11(F)].

Three-dimensional representations of 4D live embryo data (i.e., 3D + time) can be produced in one of two ways. In the first, less computationally demanding method, rotated 3D projections of image stacks are first produced using a variety of algorithms [Fig. 43.11(G,H)]. Such simple renderings can be extremely useful for identifying the 3D relationships between structures within embryos.[6] The second method, real-time, voxel-based rendering, is much more computationally demanding; for large datasets, current computing hardware accessible to the average laboratory does not permit on-demand, true real-time manipulation of the raw 4D dataset. However, once datasets are rendered, various rendering software suites permit rotation, contrast and brightness adjustment, etc., of the dataset, thereby permitting some direct manipulation of the dataset by the user [Fig. 43.11(I)]. Rendered datasets can provide striking three-dimensional views of structures within embryos (see Chapter 14, *this volume*, for further details).[7] Figures 43.1(A), 43.6(B–D), 43.7(A), 43.8(A), and 43.10(D–G) all used Volocity (Improvision, Coventry, UK) for 4D rendering. 3D + time approaches are well suited to situations in which a specimen is thick relative to its other dimensions. If the process being studied involves extensive movements of cells or relevant features along the *z*-dimension, 3D + time rendering is the method of choice.

The decision to use 2D + time versus 3D + time strategies to depict living embryos depends on several considerations. If the original raw 4D dataset does not need to be retained, 2D + time datasets require much less storage space than true 4D datasets, because they compress the data to 1/*n* its original size, where *n* is the number of focal planes in each stack. As DVD optical drives become ubiquitous, however, saving storage space is becoming less important. A second, more important practical consideration is the time required to render 3D + time datasets. For the typical end user in a developmental biology laboratory, the processing power require for ultrafast rendering of voxel-based data is financially difficult. For more typical hardware configurations, rendering of volumes from 4D datasets can take a few minutes to hours, depending on the method of rendering, the software used and the size of the original 4D dataset.

OTHER USES FOR CONFOCAL AND MULTI-PHOTON MICROSCOPY IN IMAGING AND MANIPULATING EMBRYOS

Multi-Photon–Based Ablation

Galbraith and Terasaki (2003) showed that the Ti : Sa laser in typical multi-photon microscopes can be used to cause localized damage within unlabeled cells of a sea urchin embryo via a multi-photon process (see Chapter 38, *this volume*). To intentionally generate damage, laser power was increased 10-fold, and pixel dwell time was increased 70×, that is, there was a 700× increase in total exposure. Because the multi-photon absorption events are so localized, and because the longer IR wavelengths involved penetrate more deeply into a specimen, they can produce tissue disruption at depths not possible with standard ablation laser systems. Multi-photon–induced damage is characterized by an autofluorescent scar, which allows monitoring of damage and identification of the wound site as development proceeds (see Chapter 38, *this volume*) [Fig. 43.12(A–D)].

Fluorescence Resonance Energy Transfer

The use of fluorescence resonance energy transfer (FRET) in embryos has not been reported in published journal articles, but this will likely change in the near future. FRET is becoming

[6] In addition to the built-in functions within ImageJ, which perform maximum-brightness, nearest-point, and average intensity-based 3D projections, several freeware solutions exist for rendering single time points as rotational projections within ImageJ. These include VolumeJ, by M. Abramoff (http://bij.isi.uu.nl/vr.htm), and the Volume Browser plug-in, by K. U. Barthel, which allows volumes to be manipulated in 3D (http://rsb.info.nih.gov/ij/plugins/volume-viewer.html). I have written a series of ImageJ plug-ins for batch rendering of rotational projections of embryos, available at http://worms.zoology.wisc.edu/QT4D.html. As currently written, these plug-ins support various kinds of 4D datasets, including .PIC, .AVI and .TIF image stacks, and output rotated datasets as sequential TIFF images suitable for compression using QT4DWriter.

[7] Several commercial solutions exist for 4D visualization. These include (1) Volocity from Improvision (http://improvision.com); (2) Imaris, from Bit-Plane AG (http://www.bitplane.com/); and (3) FluVR, from Scientific Volume Imaging B.V. (http://www.svi.nl/products/software/). The latter offers a free program for single-time-point surface rendering, FreeSFP, which can yield excellent rendered views of certain kinds of fluorescent signals within embryos. Freeware programs include (1) Voxx (Clendenon *et al*., 2002; http://www.nephrology.iupui.edu/imaging/voxx/), which allows freehand manipulation of rendered 3D + time data, manipulation of multi-channel data, the ability to render data as anaglyph stereo projections, and export of animations to several file formats that can be easily converted to QuickTime movies. (2) VisBio (Rueden *et al*., 2004; http://www.loci.wisc.edu/visbio/), a Java-based biological visualization tool that emphasizes data discovery and analysis, which can perform slices within 3D datasets and can perform various measurements on the data as well. VisBio's visualization capabilities are more limited in some senses than those of Voxx, but VisBio has superior slicing and interactive measurements capabilities. Because both load datasets into RAM, their memory requirements are demanding.

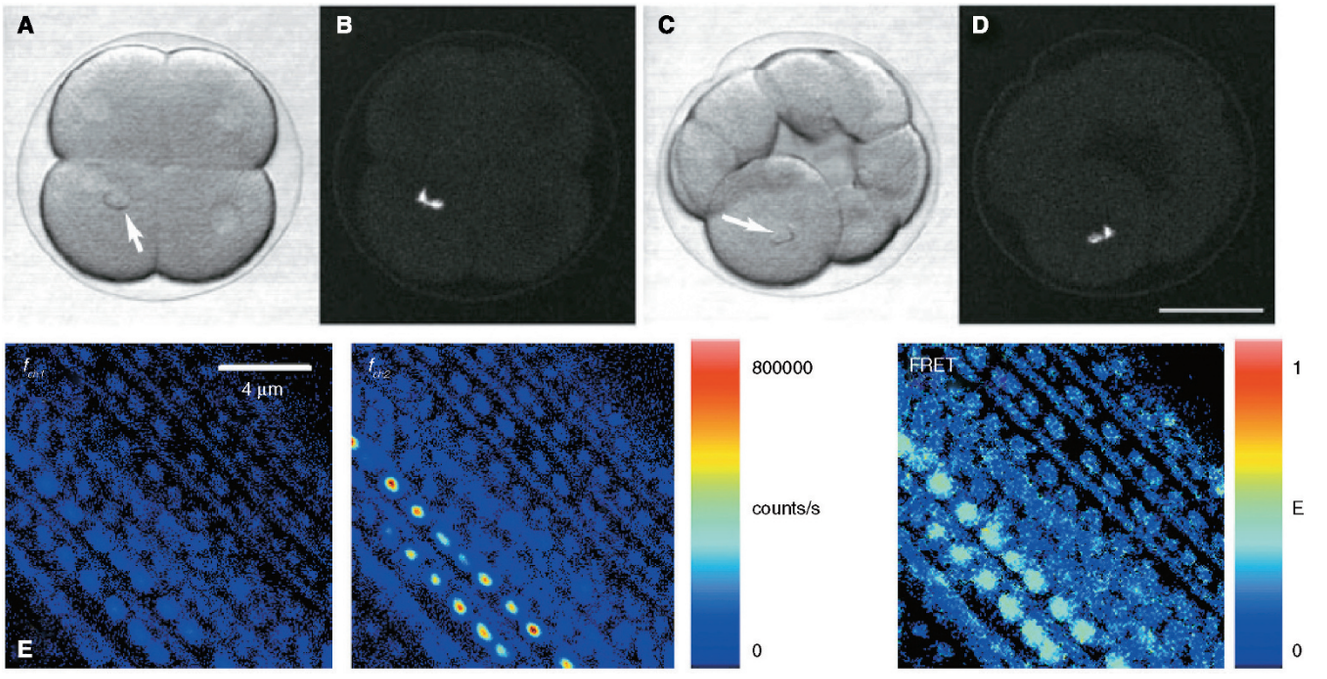

FIGURE 43.12. Multi-photon microscopy can be used to produce controlled damage and to detect protein interactions. (A–D) Damage to a mitotic pole in a sea urchin embryo. (A) Multi-photon damage was made in a two-cell stage sea urchin embryo, using a Zeiss LSM 510 MPLSM (Ti : Sa laser; *arrow*); subsequent development was observed using a Bio-Rad MRC-600 CLSM. Scanning transmission images (A, C) were obtained simultaneously with fluorescence images (B, D; 488 nm excitation) to visualize the fluorescent scar. The daughter cell that inherited the damage did not divide (C), whereas the undamaged daughter cell divided. Bar = 50 μm. (E) Two-photon excitation steady-state intensity (left, middle) and FRET efficiency (E; right) images of dense bodies in a muscle quadrant from a *C. elegans* embryo expressing PAT-4 : CFP and PAT-4 : YFP. f_{ch1}, fluorescence intensity in the CFP channel; f_{ch2}, fluorescence intensity in the YFP channel. FRET efficiency is on the order of ~30%, indicating that PAT-4 protein can self-associate in muscle dense bodies. For details of the procedure, please consult. Breusegem (2002). [A–D are from Galbraith and Terasaki (2003); (E) is from Breusegem (2002), Used by permission.]

increasingly accepted as a method for determining when two subunits of the same proteins interact with one another (intramolecular FRET) or where and when two different proteins physically interact *in vivo* (intermolecular FRET; see Chapter 45, *this volume*). Given their optical-sectioning capabilities, CLSM and MPLSM are potentially well suited to performing and imaging the results of FRET in embryos, especially because currently, the most popular donor/acceptor pair is ECFP/EYFP (Sekar and Periasamy, 2003; Wallrabe and Periasamy, 2005). One issue common to both intra- and intermolecular FRET is the contribution to acceptor excitation by autofluorescence. Embryos often display significant amounts of autofluorescence at the one-photon excitation wavelengths used for FRET, creating additional non-FRET signal that can complicate the analysis of acceptor fluorophore signals. This problem can be overcome by using two-photon excitation, which has the added advantages of increased depth of penetration mentioned previously. Breusegem (2002) reported that excitation at 850 to 870 nm reduces autofluorescence in *C. elegans* embryos.

At the time this chapter was written, no published studies had reported the use of intramolecular FRET in living embryos. However, the use of such intramolecular FRET reporters, which now includes a variety of reporters for signaling events, such as the chameleons for assessing calcium dynamics (Miyawaki *et al.*, 1999) and various reporters for small GTPase activity (Pertz and Hahn, 2004), will likely become more widespread in living embryos as the technology becomes less expensive and more widely available. One published example of intramolecular FRET using chameleons measured calcium dynamics in living *C. elegans* adults (Kerr *et al.*, 2000), suggests it has tremendous promise. Because chameleons are fusion proteins containing CFP and YFP in the same protein, the donor : acceptor ratio is always 1 : 1, so many of the complications that plague intermolecular FRET are largely obviated. This successful use of an intramolecular FRET reporter suggests that in the near future similar experiments will be performed on living embryos.

Performing intermolecular FRET in living embryos presents several additional challenges beyond those associated with intramolecular FRET. In the simplest cases, intermolecular FRET may simply be used qualitatively to show that there is an interaction between two molecules *in vivo*, after suitable correction for spectral bleed-through, but without additional computation (Wallrabe and Periasamy, 2005). In such cases, the stoichiometry of the acceptor and donor fluorophores is usually known, and FRET is reflected in changes in the ratio of both acceptor and donor emission.

However, the power of intermolecular FRET lies in the ability to use the percent energy transfer efficiency (*E%*) as a measure of intermolecular distance, that is, as a spectroscopic ruler. Quantitative FRET is much more complicated in practice than qualitative FRET, and this complication is exacerbated in living embryos. First, it is important to carefully control the concentrations of the donor and acceptor molecules for any quantitative assessment of *E%*. In transgenic animals into which fluorescent-protein-tagged molecules have been introduced, careful measurement of fluorophore concentration is difficult at best. However, in some genetic

systems, it is possible to replace the endogenous gene with a fluorescent-protein-tagged version, ensuring that virtually all of the protein under consideration is tagged. If the replacement gene is integrated as a single copy, it will typically preserve the normal level of expression of the labeled protein. A second problem with intermolecular FRET is that photobleaching of the donor or acceptor fluorophore is often used as a separate demonstration that FRET has occurred. However, photobleaching may not be suitable for embryos, many of which are especially sensitive to photodamage. An alternative is to use fluorescence lifetime imaging (FLIM) to measure FRET efficiency (Clegg *et al*., 2003; see also Chapter 27, *this volume*). FLIM has the advantage that it can be used independent of a measurement of fluorophore concentration, because the donor fluorescence lifetime decreases in the presence of FRET irrespective of fluorophore concentration. This solution introduces a third complication, however. In addition to the substantial complexities of instrumentation, quantitative determination of FRET efficiency using FLIM usually requires the acquisition of several images, which can increase the likelihood of photodamage to the embryo. For thorough quantitative FRET analysis, FLIM is often performed on a pixel-by-pixel basis throughout the field of view, increasing this risk.

Despite these caveats, recent work by Breusegem and colleagues has shown that quantitative FRET can be successfully adapted for use in *C. elegans* embryos (Breusegem, 2002). They showed that that the integrin-linked kinase (ILK), PAT-4, will engage in FRET with itself, and with both PAT-3/β-integrin and PAT-6/actopaxin at muscle dense bodies [structures associated with the attachment of muscles to the epidermis in *C. elegans*; Fig. 43.12(E)]. FRET was confirmed in several different ways, including sensitized YFP emission, and *E%* was measured using both the acceptor and donor photobleaching techniques and by performing FLIM in the time and frequency domains. In the time domain, photons were accumulated by repeated imaging of the same field at 100 µs/pixel, which required 25 to 30 frames to collect >100 photons/pixel. Although such photon-counting methods place severe limits on acquisition speed, because dense bodies are stable structures and, hence, essentially motionless, sampling of discrete points is an adequate substitute for full-field sampling, and this reduces the likelihood of phototoxicity (Breusegem, 2002). Although the use of FRET in embryos is in its infancy, these results suggest that in the near future this imaging tool, the use of which was once exclusive to cell biologists working on flat cells in tissue culture, will soon be available to developmental biologists.

CONCLUSIONS: A BRIGHT FUTURE FOR 3D IMAGING OF LIVING EMBRYOS

Few disciplines within biology have benefited more from improvements in confocal, multi-photon, and related technologies than developmental biology. As more exotic probes are developed for use in living cells, particularly those that can be genetically encoded, the imaging of embryos will continue to become more sophisticated. As each new probe is developed, there may be new challenges for developmental biologists, but based on current imaging modalities, several generalizations will probably continue to hold true.

First, although there are times when more expensive equipment, such as multi-photon microscopes, 4D deconvolution microscopes, or high-speed imaging approaches are necessary, empirical tests of viability using off-the-shelf confocal equipment should be performed first before such equipment is assumed to be necessary. While similar experiments are now being performed using multi-photon microscopy, numerous published experiments indicate that both standard single-beam confocal microscopes and disk-scanning microscopes can often be used to image living embryos in four dimensions without the need for additional equipment.

Second, as computer processing speed continues to increase, deconvolution and 3D projection of 4D datasets will become more routine. This can only improve the ability of the developmental biologist to visualize complex processes in four dimensions. The more routine use of multi-wavelength probes will likewise improve the ability of the developmental biologist to perceive and comprehend the complex beauty of embryogenesis.

Finally, although there has typically been a lag between the application of new imaging modalities in cultured cells and their subsequent use in embryos, the history of the field suggests that eventually many of the approaches first worked out in cultured cells will be adapted for use in embryos. Extension of the successful combination of microsurgical methods and confocal and multi-photon methods presented in this chapter, which effectively make the embryo flatter, will likely allow techniques such as FRET to be used routinely in embryos in the near future. Ultimately, 4D live imaging of fluorescent probes in embryos will cease to be the preserve of the specialist, and will become a part of the standard repertoire of the developmental biologist.

ACKNOWLEDGMENTS

I thank the editor of this volume and my wife, Susie, for their remarkable patience as this work was completed. I am grateful to Brian Burkel and Bill Bement for sharing unpublished data regarding PA-GFP, and to Sophie Breusegem and Bob Clegg for sharing unpublished results regarding FRET in *C. elegans*. Tim Walston, Mark Sheffield, and Chris Lockwood provided movies and images used in this work, and other members of the Hardin laboratory provided moral support. This work was supported by NIH grant GM058038 and NSF grant IBN-0112803, awarded to the author. CLSM footage was generated using a Bio-Rad 1024 confocal microscope originally purchased by NSF grant 9724515 awarded to J. Pawley. Movies associated with this chapter will be available on the Web site associated with this publication. http://www.springer.com/0-387-25921-X.

REFERENCES

Beck, J.C., Murray, J.A., Willows, A.O., and Cooper, M.S., 2000, Computer-assisted visualizations of neural networks: Expanding the field of view using seamless confocal montaging. *J. Neurosci. Methods* 98:155–163.

Bement, W.M., Sokac, A.M., and Mandato, C.A., 2003, Four-dimensional imaging of cytoskeletal dynamics in *Xenopus* oocytes and eggs, *Differentiation* 71:518–527.

Benink, H.A., and Bement, W.M., 2005, Concentric zones of active RhoA and Cdc42 around single cell wounds, *J. Cell Biol.* 168:429–439.

Benink, H.A., Mandato, C.A., and Bement, W.M., 2000. Analysis of cortical flow models *in vivo*, *Mol. Biol.1 Cell* 11:2553–2563.

Bloor, J.W., and Kiehart, D.P., 2002, *Drosophila* RhoA regulates the cytoskeleton and cell-cell adhesion in the developing epidermis, *Development* 129:3173–3183.

Breusegem, S.Y., 2002, *In vivo* investigation of protein interactions in *C. elegans* by Forster resonance energy transfer microscopy, Ph. D. dissertation, University of Illinois, Urbana-Champaign.

Campbell, R.E., Tour, O., Palmer, A.E., Steinbach, P.A., Baird, G.S., Zacharias, D.A., and Tsien, R.Y., 2002, A monomeric red fluorescent protein, *Proc. Natl. Acad. Sci. USA* 99:7877–7882.

Centonze, V.E., and White, J.G., 1998, Multiphoton excitation provides optical sections from deeper within scattering specimens than confocal imaging, *Biophys. J.* 75:2015–2024.

Chalfie, M., Tu, Y., Euskirchen, G., Ward, W.W., and Prasher, D.C., 1994, Green fluorescent protein as a marker for gene expression, *Science* 263:802–805.

Chapman, S.C., Collignon, J., Schoenwolf, G.C., and Lumsden, A., 2001, Improved method for chick whole-embryo culture using a filter paper carrier, *Dev. Dyn.* 220:284–289.

Chong, F.K., Coates, C.G., Denvir, D.J., McHale, N.G., Thornbury, K.D., and Hollywood, M.A., 2004, Optimization of spinning disk confocal microscopy: Synchronization with the ultra-sensitive EMCCD, *Proc. SPIE* 5324:65–76.

Chudakov, D.M., Belousov, V.V., Zaraisky, A.G., Novoselov, V.V., Staroverov, D.B., Zorov, D.B., Lukyanov, S., and Lukyanov, K.A., 2003, Kindling fluorescent proteins for precise *in vivo* photolabeling, *Nat. Biotechnol.* 21:191–194.

Clegg, R.M., Holub, O., and Gohlke, C., 2003, Fluorescence lifetime-resolved imaging: Measuring lifetimes in an image, *Methods Enzymol.* 360:509–542.

Clendenon, J.L., Phillips, C.L., Sandoval, R.M., Fang, S., and Dunn, K.W., 2002, Voxx: A PC-based, near real-time volume rendering system for biological microscopy, *Am. J. Physiol. Cell Physiol.* 282:C213–C218.

Cockell, M.M., Baumer, K., and Gonczy, P., 2004, lis-1 is required for dynein-dependent cell division processes in *C. elegans* embryos, *J. Cell Sci.* 117:4571–4582.

Concha, M.L., and Adams, R.J., 1998, Oriented cell divisions and cellular morphogenesis in the zebrafish gastrula and neurula: A time-lapse analysis, *Development* 125:983–994.

Cooper, M.S., D'Amico, L.A., and Henry, C.A., 1999, Confocal microscopic analysis of morphogenetic movements, *Methods Cell Biol.* 59:179–204.

Cooper, M.S., Szeto, D.P., Sommers-Herivel, G., Topczewski, J., Solnica-Krezel, L., Kang, H. C., Johnson, I., and Kimelman, D., 2005, Visualizing morphogenesis in transgenic zebrafish embryos using BODIPY TR methyl ester dye as a vital counterstain for GFP, *Dev. Dyn.* 232:359–368.

Czirok, A., Rongish, B.J., and Little, C.D., 2004, Extracellular matrix dynamics during vertebrate axis formation, *Dev. Biol.* 268:111–122.

Czirok, A., Rupp, P.A., Rongish, B.J., and Little, C.D., 2002, Multi-field 3D scanning light microscopy of early embryogenesis, *J. Microsc.* 206:209–217.

DeGrauw, C.J., Frederix, P.L.T.M., and Gerritsen, H.C., 2002, Aberrations and penetration in in-depth confocal and two-photon-excitation microscopy, In: *Confocal and Two-Photon Microscopy: Foundations*, *Applications*, *and Advances* (A. Diaspro, ed.), Wiley-Liss, New York, pp. 153–169.

Dubertret, B., Skourides, P., Norris, D.J., Noireaux, V., Brivanlou, A.H., and Libchaber, A., 2002, *In vivo* imaging of quantum dots encapsulated in phospholipid micelles, *Science* 298: 1759–1762.

Edwards, K.A., Demsky, M., Montague, R.A., Weymouth, N., and Kiehart, D.P., 1997, GFP-moesin illuminates actin cytoskeleton dynamics in living tissue and demonstrates cell shape changes during morphogenesis in *Drosophila*, *Dev. Biol.* 191:103–117.

Galbraith, J.A., and Terasaki, M., 2003, Controlled damage in thick specimens by multiphoton excitation, *Mol. Biol. Cell* 14:1808–1817.

Gao, X., Yang, L., Petros, J.A., Marshall, F.F., Simons, J.W., and Nie, S., 2005, *In vivo* molecular and cellular imaging with quantum dots, *Curr. Opin. Biotechnol.* 16:63–72.

Gimlich, R.L., 1991, Fluorescent dextran clonal markers, *Methods Cell Biol.* 36:285–297.

Girdham, C.H., and O'Farrell, P.H., 1994, The use of photoactivatable reagents for the study of cell lineage in *Drosophila* embryogenesis, *Methods Cell Biol.* 44:533–543.

Gomez, T.M., and Spitzer, N.C., 1999, *In vivo* regulation of axon extension and pathfinding by growth-cone calcium transients, *Nature* 397:350–355.

Grevengoed, E.E., Loureiro, J.J., Jesse, T.L., and Peifer, M., 2001, Abelson kinase regulates epithelial morphogenesis in *Drosophila*, *J. Cell Biol.* 155:1185–1198.

Hadjantonakis, A.K., Dickinson, M.E., Fraser, S.E., and Papaioannou, V.E., 2003, Technicolour transgenics: Imaging tools for functional genomics in the mouse, *Nat. Rev. Genet.* 4:613–625.

Hammond, A.T., and Glick, B.S., 2000, Raising the speed limits for 4D fluorescence microscopy, *Traffic* 1:935–940.

Heid, P.J., Raich, W.B., Smith, R., Mohler, W.A., Simokat, K., Gendreau, S.B., Rothman, J.H., and Hardin, J., 2001, The zinc finger protein DIE-1 is required for late events during epithelial cell rearrangement in *C. elegans*, *Dev. Biol.* 236:165–180.

Heid, P.J., Voss, E., and Soll, D.R., 2002, 3D-DIASemb: A computer-assisted system for reconstructing and motion analyzing in 4D every cell and nucleus in a developing embryo, *Dev. Biol.* 245:329–347.

Hell, S., Reiner, G., Cremer, C., and Stelzer, E.H.K., 1993, Aberrations in confocal fluorescence microscopy induced by mismatches in refractive index, *J. Microsc.* 169:391–405.

Henry, C.A., Hall, L.A., Burr Hille, M., Solnica-Krezel, L., and Cooper, M.S., 2000, Somites in zebrafish doubly mutant for knypek and trilobite form without internal mesenchymal cells or compaction, *Curr. Biol.* 10:1063–1066.

Huisken, J., Swoger, J., Del Bene, F., Wittbrodt, J., and Stelzer, E.H., 2004, Optical sectioning deep inside live embryos by selective plane illumination microscopy, *Science* 305:1007–1009.

Jacinto, A., Wood, W., Balayo, T., Turmaine, M., Martinez-Arias, A., and Martin, P., 2000, Dynamic actin-based epithelial adhesion and cell matching during *Drosophila* dorsal closure, *Curr. Biol.* 10:1420–1426.

Jaffe, L.A., and Terasaki, M., 2004, Quantitative microinjection of oocytes, eggs, and embryos, *Methods Cell Biol.* 74:219–242.

Jonkman, J.E.N., and Stelzer, E.H.K., 2002, Resolution and contrast in confocal and two-photon microscopy, In: *Confocal and Two-Photon Microscopy: Foundations*, *Applications*, *and Advances* (A. Diaspro, ed.), Wiley-Liss, New York, pp. 101–125.

Keller, R., 2002, Shaping the vertebrate body plan by polarized embryonic cell movements, *Science* 298:1950–1954.

Kerr, R., Lev-Ram, V., Baird, G., Vincent, P., Tsien, R.Y., and Schafer, W.R., 2000, Optical imaging of calcium transients in neurons and pharyngeal muscle of *C. elegans*, *Neuron* 26:583–594.

Kilian, B., Mansukoski, H., Barbosa, F.C., Ulrich, F., Tada, M., and Heisenberg, C.P., 2003, The role of Ppt/Wnt5 in regulating cell shape and movement during zebrafish gastrulation, *Mech. Dev.* 120:467–476.

Köppen, M., Simske, J.S., Sims, P.A., Firestein, B.L., Hall, D.H., Radice, A.D., Rongo, C., and Hardin, J.D., 2001, Cooperative regulation of AJM-1 controls junctional integrity in *Caenorhabditis elegans* epithelia, *Nat. Cell Biol.* 3:983–991.

Kozlowski, D.J., Murakami, T., Ho, R.K., and Weinberg, E.S., 1997, Regional cell movement and tissue patterning in the zebrafish embryo revealed by fate mapping with caged fluorescein, *Biochem. Cell Biol.* 75:551–562.

Labbe, J.C., McCarthy, E.K., and Goldstein, B., 2004, The forces that position a mitotic spindle asymmetrically are tethered until after the time of spindle assembly, *J. Cell Biol.* 167:245–256.

Langenberg, T., Brand, M., and Cooper, M.S., 2003, Imaging brain development and organogenesis in zebrafish using immobilized embryonic explants, *Dev. Dyn.* 228:464–474.

Lippincott-Schwartz, J., and Patterson, G.H., 2003, Development and use of fluorescent protein markers in living cells, *Science* 300:87–91.

Lippincott-Schwartz, J., Altan-Bonnet, N., and Patterson, G.H., 2003, Photobleaching and photoactivation: Following protein dynamics in living cells, *Nat. Cell Biol.* (Suppl.):S7–S14.

Megason, S.G., and Fraser, S.E., 2003, Digitizing life at the level of the cell: High-performance laser-scanning microscopy and image analysis for *in toto* imaging of development, *Mech. Dev.* 120:1407–1420.

Michalet, X., Pinaud, F.F., Bentolila, L.A., Tsay, J.M., Doose, S., Li, J.J., Sundaresan, G., Wu, A.M., Gambhir, S.S., and Weiss, S., 2005, Quantum dots for live cells, in vivo imaging, and diagnostics, *Science* 307:538–544.

Miyawaki, A., Griesbeck, O., Heim, R., and Tsien, R.Y., 1999, Dynamic and quantitative Ca2+ measurements using improved cameleons, *Proc. Natl. Acad. Sci. USA* 96:2135–2140.

Miyawaki, A., Sawano, A., and Kogure, T., 2003, Lighting up cells: Labelling proteins with fluorophores, *Nat. Cell Biol.* (Suppl.):S1–S7.

Mohler, W.A., 1999, Visual reality: using computer reconstruction and animation to magnify the microscopist's perception, *Mol. Biol. Cell* 10:3061–3065.

Mohler, W.A., Simske, J.S., Williams-Masson, E.M., Hardin, J.D., and White, J.G., 1998, Dynamics and ultrastructure of developmental cell fusions in the *Caenorhabditis elegans* hypodermis, *Curr. Biol.* 8:1087–1090.

Molecular Probes, 2004, *The Handbook — A Guide to Fluorescent Probes and Labeling Technologies*. Carlsbad, CA: Invitrogen Corp.

Molyneaux, K.A., Zinszner, H., Kunwar, P.S., Schaible, K., Stebler, J., Sunshine, M.J., O'Brien, W., Raz, E., Littman, D., Wylie, C., and Lehmann, R., 2003, The chemokine SDF1/CXCL12 and its receptor CXCR4 regulate mouse germ cell migration and survival, *Development* 130:4279–4786.

Oegema, K., Desai, A., Rybina, S., Kirkham, M., and Hyman, A.A., 2001, Functional analysis of kinetochore assembly in *Caenorhabditis elegans*, *J. Cell Biol.* 153:1209–1226.

Paddy, M.R., Saumweber, H., Agard, D.A., and Sedat, J.W., 1996, Time-resolved, *in vivo* studies of mitotic spindle formation and nuclear lamina breakdown in *Drosophila* early embryos, *J. Cell Sci.* 109:591–607.

Patterson, G.H., and Lippincott-Schwartz, J., 2002, A photoactivatable GFP for selective photolabeling of proteins and cells, *Science* 297:1873–1877.

Periasamy, A., Skoglund, P., Noakes, C., and Keller, R., 1999, An evaluation of two-photon excitation versus confocal and digital deconvolution fluorescence microscopy imaging in *Xenopus* morphogenesis, *Microsc. Res. Tech.* 47:172–181.

Pertz, O., and Hahn, K.M., 2004, Designing biosensors for Rho family proteins — Deciphering the dynamics of Rho family GTPase activation in living cells, *J. Cell Sci.* 117:1313–1318.

Poteryaev, D., Squirrell, J.M., Campbell, J.M., White, J.G., and Spang, A., 2005, Involvement of the actin cytoskeleton and homotypic membrane fusion in ER dynamics in *C. elegans*, *Mol. Biol. Cell*. 16:2139–2153.

Rueden, C., Eliceiri, K.W., and White, J.G., 2004, VisBio: A computational tool for visualization of multidimensional biological image data, *Traffic* 5:411–417.

Sekar, R.B., and Periasamy, A., 2003, Fluorescence resonance energy transfer (FRET) microscopy imaging of live cell protein localizations, *J. Cell Biol.* 160:629–633.

Shaner, N.C., Campbell, R.E., Steinbach, P.A., Giepmans, B.N., Palmer, A.E., and Tsien, R.Y., 2004, Improved monomeric red, orange and yellow fluorescent proteins derived from Discosoma sp. red fluorescent protein, *Nat. Biotechnol.* 22:1567–1572.

Skop, A.R., Bergmann, D., Mohler, W.A., and White, J. G., 2001, Completion of cytokinesis in *C. elegans* requires a brefeldin A-sensitive membrane accumulation at the cleavage furrow apex, *Curr. Biol.* 11:735–746.

Squirrell, J.M., Wokosin, D.L., White, J.G., and Bavister, B.D., 1999, Long-term two-photon fluorescence imaging of mammalian embryos without compromising viability, *Nat. Biotechnol.* 17:763–767.

Strickland, L., von Dassow, G., Ellenberg, J., Foe, V., Lenart, P., and Burgess, D., 2004, Light microscopy of echinoderm embryos, *Methods Cell Biol.* 74:371–409.

Strome, S., Powers, J., Dunn, M., Reese, K., Malone, C. J., White, J., Seydoux, G., and Saxton, W., 2001, Spindle dynamics and the role of gamma-tubulin in early *Caenorhabditis elegans* embryos, *Mol. Biol. Cell* 12:1751–1764.

Terasaki, M., 1998, Imaging of echinoderm fertilization, *Mol. Biol. Cell* 9:1609–1612.

Terasaki, M., and Jaffe, L.A., 2004, Labeling of cell membranes and compartments for live cell fluorescence microscopy, *Methods Cell Biol.* 74:469–489.

Thomas, C., DeVries, P., Hardin, J., and White, J., 1996, Four-dimensional imaging: Computer visualization of 3D movements in living specimens, *Science* 273:603–607.

Thomas, C.F., and White, J.G., 2000, Acquisition, display, and analysis of digital three-dimensional time-lapse (four-dimensional) data sets using free software applications, *Methods Mol. Biol.* 135:263–276.

Ulrich, F., Concha, M.L., Heid, P.J., Voss, E., Witzel, S., Roehl, H., Tada, M., Wilson, S.W., Adams, R.J., Soll, D.R., and Heisenberg, C.P., 2003, Slb/Wnt11 controls hypoblast cell migration and morphogenesis at the onset of zebrafish gastrulation. *Development* 130:5375–5384.

Voie, A.H., Burns, D.H., and Spelman, F.A., 1993, Orthogonal-plane fluorescence optical sectioning: three-dimensional imaging of macroscopic biological specimens. *J. Microsc.* 170:229–236.

Wallrabe, H., and Periasamy, A., 2005, Imaging protein molecules using FRET and FLIM microscopy, *Curr. Opin. Biotechnol.* 16:19–27.

Wilson, P., and Keller, R., 1991, Cell rearrangement during gastrulation of *Xenopus*: Direct observation of cultured explants, *Development* 112:289–300.

Wood, W., and Jacinto, A., 2004, Imaging cell movement during dorsal closure in *Drosophila* embryos, *Methods Mol. Biol.* 294:203–210.